www.sciencemag.org/cgi/content/full/science.aaa1975/DC1

Supplementary Materials for

Human-specific gene *ARHGAP11B* promotes basal progenitor amplification and neocortex expansion

Marta Florio, Mareike Albert, Elena Taverna, Takashi Namba, Holger Brandl, Eric Lewitus, Christiane Haffner, Alex Sykes, Fong Kuan Wong, Jula Peters, Elaine Guhr, Sylvia Klemroth, Kay Prüfer, Janet Kelso, Ronald Naumann, Ina Nüsslein, Andreas Dahl, Robert Lachmann, Svante Pääbo, Wieland B. Huttner*

*Corresponding author. E-mail: huttner@mpi-cbg.de

Published 26 February 2015 on *Science* Express
DOI: 10.1126/science.aaa1975

This PDF file includes:

Other Supplementary Material for this manuscript includes the following:
(available at www.sciencemag.org/cgi/content/full/science.aaa1975/DC1)

Tables S1, S2, and S4 (Excel files)

Florio et al., Supplementary Materials

Materials and Methods

Mice. All experimental procedures were designed and conducted in agreement with the German Animal Welfare Legislation. Animals used for this study were kept pathogen-free at the Biomedical Services Facility (BMS) of the MPI-CBG. All mice used, wild-type (wt), Tis21::GFP knock-in (*36*) or Tubb3-GFP transgenic (*21*), were congenic and C57BL/6JOlaHsd. Embryonic day (E) 0.5 was set at noon of the day on which the vaginal plug was observed. Unless otherwise specified, all experiments were performed in the dorsolateral neocortex of E13.5-E14.5 embryos, and all images acquired and analysed from coronal sections of the prefrontal and parietal neocortex.

Human tissue. Human fetal brain tissue was obtained from the Klinik und Poliklinik für Frauenheilkunde und Geburtshilfe, Universitätsklinikum Carl Gustav Carus of the Technische Universität Dresden, following elective pregnancy termination and informed written maternal consents, and with approval of the local University Hospital Ethical Review Committees. The age of fetuses ranged from 12 to 13 wpc (12 wpc, $n = 1$; 13 wpc, $n = 2$) as assessed by ultrasound measurements of crown-rump length and other standard criteria of developmental stage determination. Human fetuses were placed on ice immediately after abortion and neocortices were dissected in ice-cold Tyrode's Solution (TS) and either processed for DiI labeling or fixed for at least 3 h at room temperature followed by 24 h at 4°C in 4% PFA in 120 mM phosphate buffer (pH 7.4). The 16 wpc human brain used for immunofluorescence analyses (shown in Fig. S8) was obtained from Novogenix Laboratories (Torrance, CA), following informed consent and elective termination. Developmental age was determined by ultrasound.

DiI labeling.

DiI solution. For DiI labeling, a 2 mM DiI working solution was prepared as follows: DiI crystals (Molecular Probes, D-3911) were dissolved in DMSO (Sigma) to a final concentration of 2 mg/ml in 1 ml final volume. The resulting solution was mixed by vortexing until no crystals were visible, and then centrifuged at 16,000 x g, for 30 min at room temperature. The supernatant was transferred to a new Eppendorf tube and stored in the dark at room temperature for a maximum of 1 month.

DiI labeling for NPC isolation. In mouse NPC isolation experiments, the following E14.5 mice were used: wt, *Tubb3*-GFP transgenic or *Tis21*::GFP heterozygous. For each experiment, 1-3 litters were used and pooled together. Embryonic brains were dissected in ice-cold TS and screened for GFP fluorescence under an epifluorescent stereomicroscope (SZX16 Olympus). Up to 4 GFP+ and 2 GFP– brains were collected. In experiments performed with the *Tubb3*-GFP mice, GFP– and GFP+ brains were dissected from littermate embryos, whereas in experiments with the *Tis21*::GFP mice, GFP– brains were dissected from E14.5 embryos of a wt litter.

Next, the cerebral hemispheres were separated from each other and the meninges removed from the dorsolateral cortex. After dissection, hemispheres were kept on ice until further processed, one by one, as follows. Each hemisphere was transferred to a petri dish filled with 10-15 ml of pre-warmed (37°C) TS, and DiI was applied to the basal surface of the dorsolateral cortex by means of a mouth-controlled pipette-tip, lightly brushing against the entire surface of the cerebral tissue (10 µl per passage). After 2-3 passages, the hemisphere was quickly transferred to a new TS-filled petri dish, and unbound DiI crystals washed away by gentle rotation of the dish, after which DiI solution was applied again. Up to 5 cycles of labelling, each followed by washing, were repeated until the whole cerebral surface was uniformly coated with DiI. During the entire procedure, specificity and magnitude of labeling were visualized by epifluorescent illumination under a stereomicroscope. For FACS experiments, up to 6 *Tubb*-GFP+ or *Tis21*::GFP+ cortices were labeled; for flow cytometry analysis, the following control samples were prepared and processed in parallel: 2 DiI-labeled, GFP– cortices (DiI-only control), 2 DiI-unlabeled, GFP+ cortices (GFP-only control), 3 DiI-unlabeled, GFP– cortices (untreated control). In human NPC isolation experiments, the procedure was performed as described for mouse, with the following variation: after dissection, the 13 wpc fetal cerebral cortices were cut with a scalpel into smaller pieces of 5x5 mm, each of which was labeled individually. In each experiment, one piece was left unlabeled as a DiI-negative control for flow cytometry analysis.

After DiI application, mouse brain hemispheres and human cortical fragments, along with control samples, were transferred to 20-ml glass flasks, with one hemisphere/cortical fragment per flask and each flask containing 1.5 ml of DMEM/F12 medium (Life Technologies) supplemented with 1x N2 (Life Technologies) and 1x B27 (Life Technologies). Hemispheres and cortical fragments were cultured for 2.5 h and 4.5 h, respectively, in a whole-embryo culture incubator (HERO culture system, (*37*) at 37°C in an atmosphere of 60% O_2, 5% CO_2, 35% N_2, with continuous slow rotation at 8 rpm.

Sparse DiI labeling shown in Fig. 1 and Fig. S1, was performed as described above, but using a less concentrated DiI solution (0.2 mM), sparsely applied to the cortical tissue.

DiI diffusion rate measurements. The diffusion rate of DiI in live tissue was analyzed in the neocortex of E14.5 wt embryonic mice, as follows: individual hemispheres were dissected and DiI-labeled as described above, followed by embedding in 3% low-melting agarose (Sigma) at different time-points (1 min, 30 min, 1.5 h, 2.5 h, 3.5 h) after labeling. Immediately after embedding, 2-3 200-µm thick coronal sections from each hemisphere were cut on a Vibratome (Leica VT1000S). During cutting, agarose blocks were immersed in ice-cold PBS, to slow down the diffusion of DiI. Sections were immediately transferred to glass bottom dishes (MatTek), fixed for 5 min in 4% PFA, quickly rinsed in 1x PBS, and mounted in Mowiol 4-88 (Sigma) for microscopy analysis.

Single cell suspension. After DiI labeling, neocortices were microdissected under an epifluorescent stereomicroscope and, if present, unlabeled regions were removed. For mouse NPC isolation experiments, 4-6 DiI-labeled, *Tubb3*-GFP+ or *Tis21*::GFP+ cortices were pooled together in a 2 ml microcentrifuge tube. Cortices of each control condition were also pooled together and processed in parallel. As to human NPC isolation experiments, each cortical piece was dissociated in a separate tube and pooled before FACS (see below). Single cell suspensions

were produced using the MACS Neural Tissue Dissociation kit containing papain (Miltenyi Biotec), adapting the dissociation protocol as follows. All samples were incubated with the papain-containing solution (Enzyme Mix 1 of the kit, prepared according to the manufacturer's instructions in 1 ml final volume) for 15 min at 37°C on a rotating wheel, followed by addition of a papain inhibitor-containing solution (Enzyme Mix 2 of the kit, prepared according to the manufacturer's instructions in 15 µl final volume). Samples were then dissociated by gentle trituration (up to 10 up-and-down passages through a P-1000 tip) to obtain a single-cell suspension, collected by centrifugation at 300 x g for 3 min, and resuspended in 600 µl of TS. Cell viability was assessed using a 5 µl aliquot of the cell suspension for Trypan blue staining, and typically was 90-95%.

Prom1 cell surface staining. Cell surface staining of prominin-1 was performed on the mouse cell suspensions with rat anti-13A4-APC conjugated (1:300, eBioscience, Clone 13A4, #17-1331-81), and on the human cell suspensions with mouse-anti-CD133/1-APC conjugated (1:11; Miltenyi Biotect; #130-090-826). Cells were incubated with prominin-1 antibody on ice for 30 min in TS (up to $1x10^7$ cells per 100 µl in 300 µl final volume). Rat IgG1-APC (1:300, eBioscience, #17-4301-81) and mouse IgG1-APC (1:11; Miltenyi Biotect; #130-092-214) were used as isotype controls on mouse and human cell suspensions, respectively.

Vital DNA staining. After prominin-1 staining, human cell suspensions were collected by centrifugation at 300 x g for 5 min, resuspended in pre-warmed DMEM/F12 (Life Technologies) to $1x10^6$ cells per ml and stained with a vital DNA stain (1:1000; Vybrant DyeCycle Violet Stain, Life Technologies) for 30 min under gentle rotation at 37°C. After DNA staining, cells were collected by centrifugation at 300 x g, resuspended in TS and immediately processed for flow cytometry analysis followed by FACS.

Flow cytometry and FACS. Flow cytometry and FACS were performed on a 5-laser - BD FACSAria IIIu sorter (BD Bioscience), and analyzed using the FACS Diva software (BD Bioscience, v8.0).

Cell suspensions were passed through a filter (40-µm pore size) and kept on ice until processed for flow cytometry analysis. 20,000 events were acquired, and gates were applied as follows. First, a P1 gate was set on the SSC/FSC dot-plot, to identify live cells based on size and shape. Next, the P1 fraction was restricted by setting a P2 gate on the SSC-W/SSC-A dot-plot, to confine further analyses and sortings to single cells. Out of the P2 population, single dot-plots were created for SSC/GFP (linear/exponential, blue laser, 488 nm), SSC/PE (linear/exponential, yellow-green laser, 561 nm) and SSC/APC (linear/exponential, red laser 633 nm), to visualize the fluorescence intensity of *Tubb3*-GFP, DiI, and prom-1-APC, respectively. For human samples, histograms (linear, UV laser, 375 nm) were also generated for Hoechst Blue to visualize fluorescence of the vital DNA dye. Voltage parameters were set based on untreated and isotype controls, and subsequently maintained for FACS. Control samples containing only one fluorescent marker (DiI only, Prom1 only, *Tubb3*-GFP only and DNA dye only) were used to assess spectral overlap between channels, and red/greed compensation was applied. Finally, the following gates were restrictively set and maintained through FACS. As to experiments

performed in *Tubb3*-GFP embryos: GFP–/DiI+/Prom1+ (aRG), GFP–/DiI+/Prom1– (bRG), GFP–/DiI–/Prom1– (bIP), GFP+/DiI+/Prom1– (neurons, N_b); as to experiments performed in *Tis21*::GFP embryos: GFP–/DiI+/Prom1+ (Tis21– aRG) and GFP+/DiI+/Prom1+ (Tis21+ aRG); as to experiments performed in human fetal brains: DiI+/Prom1+/S-G2-M (aRG), DiI+/Prom1–/S-G2-M (bRG), DiI+/Prom1–/G1-G0 (neurons, N_b). For each of these fractions, 5,000 cells were sorted into microcentrifuge tubes filled with 200 µl of RLT lysis buffer (Qiagen) containing 2 µl of b-mercaptoethanol (Sigma), and stored at –80°C until further processed as indicated below. FACS was performed at 4°C, using a 100 µm nozzle. Five independent experiments each were conducted for mouse NPC isolation from E14.5 *Tubb3*-GFP and *Tis21*::GFP embryos. As to human NPC isolation, two independent experiments were conducted starting with two 13 wpc human fetal cortices, each of which was split into two samples, which were processed independently and sorted one after the other.

For single-cell qPCR analysis, individual cells were sorted, using the FACS Diva single-cell sort precision mode, into 96-well plates (Eppendorf, twin.tec, skirted, #951020486) containing 3.5 µl water with 0.25 µl 10% NP40 per well and snap-frozen. Two experiments were conducted on three E14.5 wt littermate embryos, and one acquisition was performed on one 12 wpc human fetal brain.

mRNA amplification and Next Generation Sequencing (NGS) library preparation. Total RNA was extracted using the RNAeasy Mini kit (Qiagen) according to the manufacturer's instructions. Complete cDNA was synthesized from half of the isolated mRNA with SmartScribe reverse transcriptase (Clontech) using a universally tailed poly-dT primer and template switching oligos. This was followed by amplification of the purified cDNA with the Advantage 2 DNA Polymerase (12 cycles). After ultrasonic shearing of the amplified cDNA (Covaris S2), samples were subjected to standard Illumina fragment library preparation using the NEBnext chemistries (New England Biolabs), in brief: fragments were end repaired, A-tailed and ligated to indexed Illumina Truseq adapters. Subsequently, the NGS libraries were finalized by a universally primed PCR amplification (15 cycles). Libraries were purified using XP beads (Beckman Coulter), quantified by qPCR (KAPA Biosysytems) and subjected to Illumina 75-bp single end sequencing on the Illumina HiSeq 2000 platform providing on average 35 Mio reads per sample (see Fig S4).

Transcriptome data analysis. Reads of the same sample on different sequencing lanes were combined and subjected to adapter trimming using cutadapt. The processed reads were aligned to the mouse reference genome (mm10) and the human genome (hg19), using TopHat (v2.0.11). Genes of the Ensembl release 61 were quantified using cufflinks v0.9.3(15), with the resulting RNAseq data being expressed as FPKM values. Orthologous genes were assigned based on annotated Ensembl one-to-one orthologs. Replicates were clustered using Jensen–Shannon divergence. For mouse, the most distant replicate for aRG, bRG, bIP and neurons was identified and discarded. For human, two neurons samples, one in each experiment were discarded. Differential expression analysis was performed using cuffdiff (v2.2.1) with FPKM values as data input, and using all protein-coding genes as transcriptome reference. We performed this analysis for the sum of all transcripts present for any given gene, and did not distinguish between different transcripts (splice variants). Expressed genes were defined using a cutoff of FPKM >1.

Differentially expressed genes were defined using a cutoff of $p<0.01$. Numbers of differentially expressed genes in the various sectors of Venn diagrams were calculated using R (http://www.r-project.org/). Functional annotation clustering of the differentially expressed genes was performed using DAVID (http://david.abcc.ncifcrf.gov), with default settings. Data visualization was performed using Cummerbund and R (http://www.r-project.org/). Orthologous genes were assigned based on annotated Ensembl (eg version 77) one-to-one orthologs.

Gene expression analysis by RT-qPCR. Total RNA was isolated using the RNAeasy Mini kit (Qiagen) according to the manufacturer's instructions. cDNA was synthesized using random hexamers and Superscript III Reverse Transcriptase (Life Technologies). qPCR was performed using the ABsolute qPCR SYBR Green mix (Thermo Scientific) on an Mx3000P qPCR system (Agilent Technologies). Error bars represent SD of three PCR amplifications for each sample. Similar results were obtained in at least three independent experiments for mouse and two independent experiments for human. Primer sequences are provided in Table S3.

MicroRNA expression analysis by RT-qPCR. MicroRNAs were isolated using the miRNAeasy Micro kit (Qiagen) according to the manufacturer's instructions. cDNA was synthesized using the miScript II RT kit (Qiagen). qPCR was performed using the miScript SYBR Green PCR kit (Qiagen) on an Mx3000P qPCR system (Agilent Technologies). Primers for *miR92* (Mm_miR-92_1) and *miR92b* (Mm_miR-92b_1) were from Qiagen.

Gene expression analysis by single cell RT-qPCR. Total RNA was isolated as described above. For reverse transcription, 1.2 µl 5x VILO Reaction Mix and 0.3 µl SUPERase-In (Life technologies) were added, the RNA denatured at 65°C for 90 sec, followed by addition of 0.15 µl 10x SuperScript Enzyme Mix (Life technologies), 0.12 µl T4 Gene 32 protein (NEB) and 0.73 µl water, and incubation at 25°C for 5 min, 50°C for 30 min, 55°C for 25 min, 60°C for 5 min and 70°C for 10 min. Subsequently, cDNA was amplified with a gene-specific primer mix (each primer at a final concentration of 50 nM) and TaqMan PreAmp Master Mix (Life technologies) using 20 cycles of 96°C for 5 sec and 60°C for 4 min after initial enzyme activation at 96°C for 10 min. Unincorporated primers were removed by Exonuclease I (NEB) digestion. The final cDNA was diluted 5-fold prior to analysis with Sso Fast EvaGreen Supermix and gene-specific primers combined with assay loading reagent in 96.96 Dynamic Array Chips for Gene Expression on a BioMark System (Fluidigm). Ct values were calculated with the system's software (BioMark Real-time PCR Analysis; Fluidigm). Wells with below- or above-average Rox signal were excluded form the analysis. Each assay was performed in duplicate. Primer sequences are provided in Table S3. Cells with failed readings for housekeeping genes (*Gapdh, Hprt, Actb*) were excluded from the analysis. Expression values were calculated relative to *Actb*. For human, expression of cell-type specific markers for endothelial cells (*PECAM*, *EMCN*, *ICAM2*, *CDH5* and *FLT1*), microglial cells (*AIF1*, *ITGAM* and *CD68*) and oligodendrocytes (*OLIG1* and *OLIG2*) were included in the analysis to identify potential contamination by these cell types.

For unsorted cells, expression values for *Prom1* versus *Mapt* and *Prom1* versus *Dcx* were plotted. Cells with high *Prom1* and low *Mapt/Dcx* were assigned as APs, cells with low *Prom1*

and high *Mapt/Dcx* were assigned neurons (N), and everything intermediate was considered a BP (see Fig. S3). To assess the variable contribution of each gene in classifying the cell types, random forest analysis was performed in R using the *randomForest* function. The *importance* function was then used to identify the important variables for classifying the data. The mean decrease accuracy for all the variables was plotted using the *VarImpPlot* function. PCA analysis was performed in R using the principal component analysis (*prcomp*) function.

Presence of *ARHGAP11B* in the Neandertal and Denisovan genomes. To determine whether *ARHGAP11B* is present in Neandertal and/or Denisovans, we assessed whether reads carrying variants specific to *ARHGAP11A* and *ARHGAP11B* could be identified in the archaic genomes. To exclude regions that are susceptible to ambiguous alignments of the short Neandertal and Denisovan sequences, we applied the mappability track (map35_100%) developed for the Neandertal genome (*31*). Briefly, we looked for regions in *ARHGAP11A* and *ARHGAP11B* where all overlapping 35mers map uniquely when allowing for up to one mismatch in the alignment. We identified a unique region where *ARHGAP11A* and *ARHGAP11B* differ by 1 indel and 1 substitution:

```
ARHGAP11A    TAAG--CAAGAGTTAAGATGTAAAg   (chr15:32,910,822-32,910,844)
ARHGAP11B    TAAGTACAAGAGTTAAGATGTAAAa   (chr15:30,921,430-30,921,454)
```

Using only reads that are confidently aligned to these genomic regions (MQ>=30), we identified 34 reads that support the presence of *ARHGAP11A* and 29 reads in support of *ARHGAP11B* in the Altai Neandertal. In the Denisovan we identified 22 reads that support the presence of *ARHGAP11A* and 20 reads in support of *ARHGAP11B*. We therefore conclude that *ARHGAP11B* is present in both the Neandertal and the Denisovan genomes, and that the duplication of *ARHGAP11A* occurred after the split from the common ancestor with chimpanzee, and prior to the split of modern humans from the common ancestor with Neandertals and Denisovans.

RhoGAP activity assay. DNA constructs encoding myc-tagged, full-length and truncated versions of human ARHGAP11A and of ARHGAP11B were generated by standard molecular cloning. Cos7 cells were transiently transfected with pCAGGS-myc-KK1 (control), pCAGGS-myc-*ARHGAP11A*, pCAGGS-myc-*ARHGAP11A-250*, pCAGGS-myc-*ARHGAP11A-220* and/or pCAGGS-myc-*ARHGAP11B*. One day after transfection, total cell lysates were subjected to SDS-PAGE followed by immunoblot analyses with rabbit anti-myosin phosphatase target protein 1 (MYPT1) (*38*), rabbit anti-MYPT1-pT853 (Cell Signaling Technology) and mouse anti-myc (9E10, MPI-CBG) antibodies.

***In utero* electroporation.** *In utero* electroporation was performed as previously described (*39*). Pregnant wt mice carrying E13.5 embryos were deeply anesthetized using isofluorane and received a subcutaneous injection of analgesic prior to surgery. The peritoneal cavity was then surgically opened and the uterus exposed. In experiments shown in Fig. 3A-B, embryos were injected intraventricularly with 2 µg/µl of pCMV-EGFP-C1 (Clontech) and either 2 µg/µl of pCMV6-AC (Origene, PS100020) or 2 µg/µl of pCMV6-AC-ARHGAP11B (Origene, SC324558), in 1x PBS containing 0.1% fast green (Sigma). In experiments shown in Figs. 3C-E,

4C-G, the EcoRI-XhoI insert from the pCAV6-AC-ARHGAP11B was inserted into a pCAGGS vector. Embryos were injected intraventricularly with 0.3 μg/μl of pCAGGS-GFP and either 0.4 μg/μl of pCAGGS-empty or 0.4 μg/μl of pCAGGS-ARHGAP11B, in 1x PBS containing 0.1% fast green (Sigma).

Electroporations were performed with six 50-msec pulses of 30-36 V at 1 sec intervals. Embryos were harvested 24 h, 48 h or 5 days post-electroporation and PFA-fixed for immunofluorescence analysis.

It has previously been reported that *in utero* electroporation can have the side effect of displacing progenitor cells (mostly the non-electroporated subpopulation in the electroporated region) towards the cortical plate (*40*). To avoid this artifact from becoming relevant for our data showing an increase in mouse basal progenitors upon *ARHGAP11B* expression (Fig. 3), we have only considered those experiments in which the effect of *ARHGAP11B* expression occurred only in the progeny of electroporated cells (i.e., GFP+ cells) and in which there was little or no effect on GFP– cells. We observed an increased appearance of non-electroporated progenitor cells in the SVZ and intermediate zone in some control-electroporated and some *ARHGAP11B*-electroporated regions, although seemingly more frequently upon *ARHGAP11B* electroporation. This raises the possibility that *ARHGAP11B* expression may increase basal progenitors also via a non-cell autonomous effect, an issue that requires further investigation.

Microinjection

In-vitro transcription. pTNT-mRFP and pCMV6-AC-ARHGAP11B plasmids were linearized using NotI and SacII, respectively. Capped and polyadenylated mRFP and ARHGAP11B RNA was obtained by *in vitro* transcription using the T7 mMESSAGE-mMACHINE Ultra kit (Ambion). IVT-RNA was dissolved in RNase-free bidistilled water (1 μg/μl), snap-frozen and kept at -80°C.

Slice preparation. E14.5 telencephalon was dissected at room temperature in TS pre-warmed at 37°C. After removal of meninges, telencephalon was immersed in 3% low-melting agarose (Agarose Type XI, Sigma) in 1x PBS at 37°C. After solidification of the agarose, 250 μm slices were cut using a vibratome (Leica VT1000S, Leica). Slices were transferred to 3.5-cm dishes containing 37°C-warm slice-culture medium (SCM), consisting of Neurobasal medium (Gibco) supplemented with 10% rat serum (Charles River Japan), 2 mM L-glutamine (Gibco), Penstrep (Gibco), N2 supplement (17502-048, Invitrogen), B27 supplement (17504-044, Invitrogen) and 10 mM Hepes-NaOH pH 7.3.

Microinjection. Microinjection was performed as described previously (*32*). Brain slices were transferred to 3.5 cm dishes containing 37°C-warm CO_2-independent microinjection medium (CIMM), consisting of DMEM-F12 (Sigma D2906) containing 2 mM L-glutamine, Penstrep, N2 and B27 supplements, and 25 mM (final concentration) Hepes-NaOH pH 7.3, and kept at 37°C on a heated stage during microinjection. Microinjection was performed using the manual mode and a compensation pressure of 100-200 hPa.

The microinjection solution contained in vitro transcribed RFP RNA (0.3 μg/μl) without or with in vitro transcribed ARHGAP11B RNA (0.3 μg/μl) and Dextran-3000-Alexa488 as a tracer (3.3 μg/μl). RNA was heated to 90°C for 30–45 sec and cooled to 4°C prior to the addition of the dextran tracer. Microinjection solutions were centrifuged at 16,000 g for 30 min at 4°C, and the

supernatant was collected, kept on ice and used for microinjection. After microinjection, slices were embedded in collagen as described and kept in culture for 24 or 48 h in the slice-culture incubator at 37°C, with 40% O_2 before PFA fixation.

Immunofluorescence. Immunofluorescence was performed either on 50-70 µm vibratome sections or on 25 µm cryosections, as follows. Antigen retrieval was performed in 0.01 M citrate buffer for 1 h at 70°C. Sections were then permeabilized with 0.1% Triton X-100 in PBS for 30 min, quenched with 0.1 M glycine in PBS for 30 min, followed by blocking, primary and secondary antibody incubations, and washings in 1x PBS containing 0.2% gelatin, 150 mM NaCl and 0.3% Triton X-100. Primary antibodies were incubated overnight at 4°C and secondaries for 2 h at room temperature. Sections were mounted in Mowiol 4-88.

For immunofluorescence performed on DiI-labeled tissue (shown in Fig. 1C-D' and Fig. S1A-C), 100-µm vibratome sections were permeabilized with 1 mg/ml digitonin (rather than Triton X-100) in 3% BSA in PBS, followed by blocking, primary and secondary antibody incubations in the same medium. For immunofluorescence performed on DiI-labeled cell suspensions (shown in. Fig. S1H, cells were plated on poly-D-lysine-coated coverslips in a 24-well plate, with 50,000 cells per well, and left to adhere for 3 h at 37°C in a cell culture incubator before fixation in 4% PFA for 30 min in ice, followed by immunostaining as described above.

For immunofluorescence of prominin-1 as shown in Fig.1F, cells were subjected to prominin-1 cell surface staining and then plated at 300,000 cells per well (5 mm diameter) on adhesive slides (Marienfeld GmbH) and left to adhere for 15 min in DMEM/F12 containing donkey anti-rat-Alexa488 (1:500; Life Technologies) and Hoechst DNA stain (1:5,000). Cells were fixed with 2% PFA for 10 min and mounted in Mowiol 4-88.

Antibodies. Mouse: mAb anti phosphovimentin (Abcam, ab22651), rabbit: pAb anti Pax6 (Covance, PRB-278P); pAb anti Tbr2 (Abcam, ab23345); rat, Ab Anti-Histone H3 (phospho S10, ab10543); goat: antibody anti EGFP (MPI-CBG); chicken: Tbr2 (Millipore, AB15894), GFP (Aves labs, GFP-1020), RFP (ChromoTek, 5F8). Secondary antibodies: donkey anti goat Alexa 488, donkey anti rabbit Alexa 647, donkey anti Mouse Alexa 555 (Life technologies), Donkey anti Rat Cy3, Donkey anti Chicken Cy5 (Jackson Laboratories). DNA staining: DAPI (Sigma).

Image acquisition. Confocal images were acquired using a LSM 700 inverted microscope (Zeiss) or a LSM 510 (Zeiss). Stacks of typically 1024 × 1024 pixels × 15-40 2-µm optical sections were acquired. Images were analysed and processed with ImageJ (http://imagej.nih.gov/ij/).

Statistics. Cell counts were analysed using Excel (Microsoft) and results visualized using Prism (GraphPad Software). Statistical tests used: paired and unpaired Student's *t*-test. For details relevant to the statistical analyses, see the Table S3.

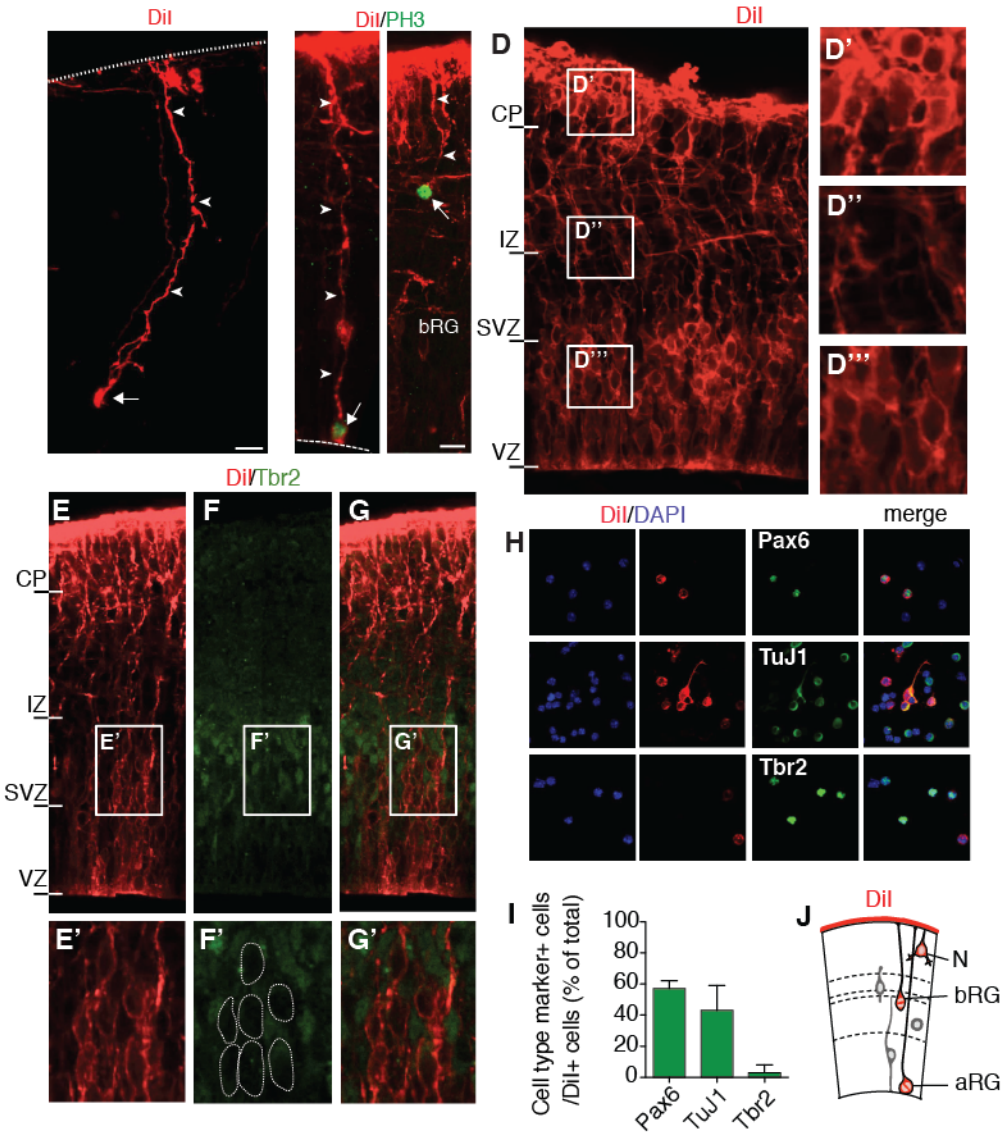

Fig. S1: DiI labeling is specifically confined to cells contacting the basal lamina.

(**A-C**) Sparse DiI labeling of E14.5 mouse neocortex from the basal lamina (dotted lines), combined with phosphohistone H3 (PH3) immunofluorescence (green; **B**, **C**). Arrows, cell body; solid arrowheads, basal process; open arrowhead, apical process; dashed lines, ventricular surface. Note the mitotic aRG in (**B**) and the mitotic bRG in (**C**). (**D**) Coronal section of an E14.5 mouse neocortex labeled by DiI, showing the cell bodies of aRG located in the VZ (**D'''**) and N_b in the basal-most region of the CP (**D'**), but virtually no cell bodies of bIPs or migrating neurons in the SVZ and IZ (**D''**). (**E-G**) Immunofluorescence staining for Tbr2 performed on a 70 µm vibratome section from a DiI-labeled E14.5 mouse neocortex, showing virtually no overlap between Tbr2 and DiI in the basal part of the VZ and SVZ. Boxes indicate insets shown a higher magnification in the bottom panels (**E'-G'**). Dashed lines in (**F'**) indicate cell bodies. (**H-I**) Immunofluorescence stainings (**H**) for Pax6 (top row), TuJi1 (middle row) and Tbr2 (bottom row) performed on a single-cell suspension prepared as described in Fig. 1 from a pool of 4 DiI labeled mouse neocortices (E14.5). (**I**) Proportions of each marker are plotted and expressed as percentage of total DiI+ labeled cells in the suspension. Note that only 4% of DiI+ cells stain positive for Tbr2. Data are the mean of 3 microscopy fields. Bars represent the SD. (**J**) Cartoon showing the three cell types to which basal DiI labeling is confined.

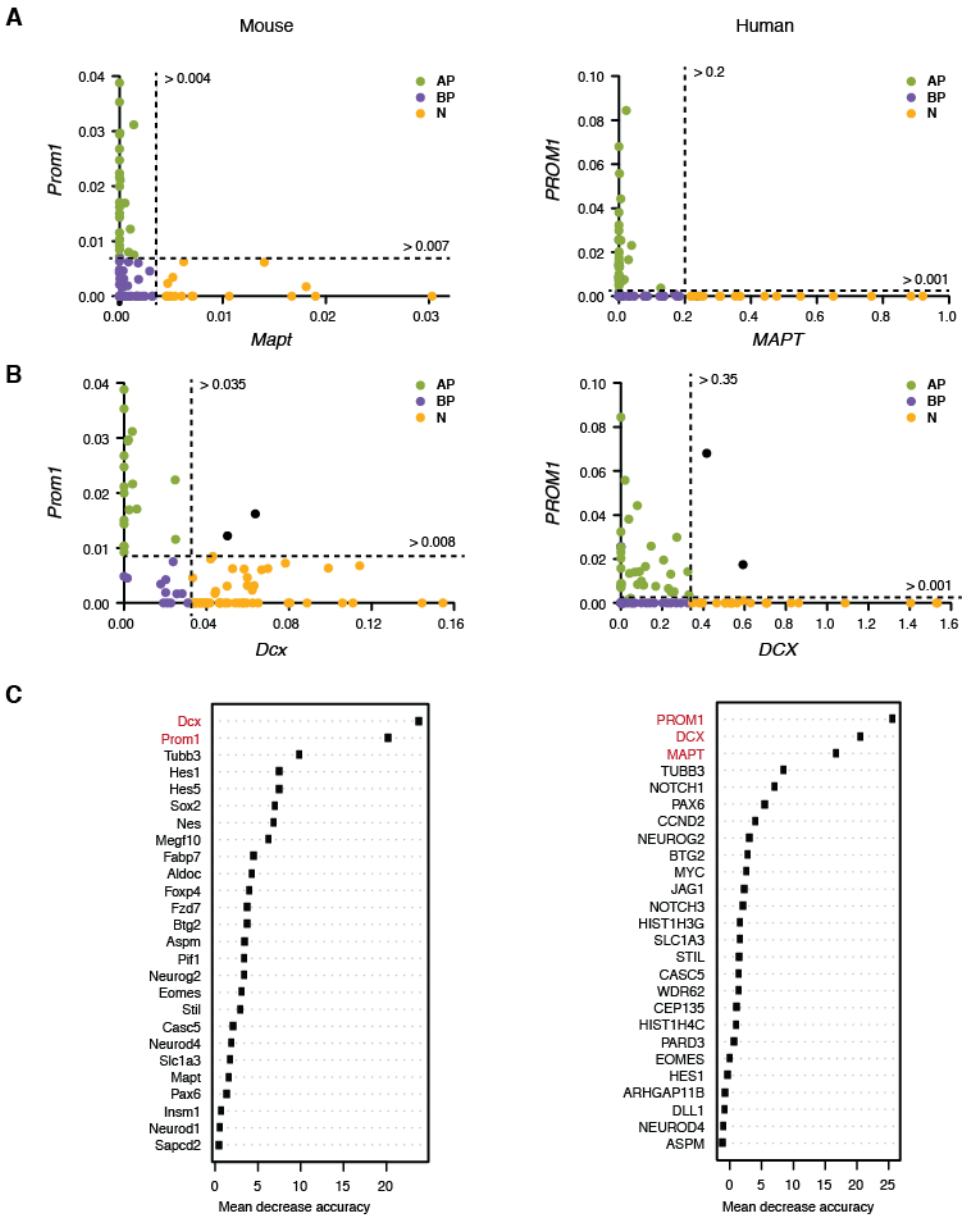

Fig. S2: Classification of unsorted cortical cells after single cell RT-qPCR.

Single cell RT-qPCR was performed on unsorted mouse and human cortical cells to validate the results obtained using the purification method described in Fig. 13. Following the analysis, cells were retrospectively classified as APs, BPs or neurons (N). (**A**) *Prom1* expression was plotted against *Mapt* expression for mouse (left) and human (right). Each dot represents an individual cell. Cut-offs used for cell type assignment are indicated. (**B**) *Prom1* expression plotted against *Dcx* expression. Cells highlighted in black do not match any of the groups and were excluded from the analysis. (**C**) To assess the variable importance of each gene in classifying the cell types, random forest analysis was performed and the mean decrease accuracy for all variables plotted. The genes that contribute most to the classification are highlighted in red.

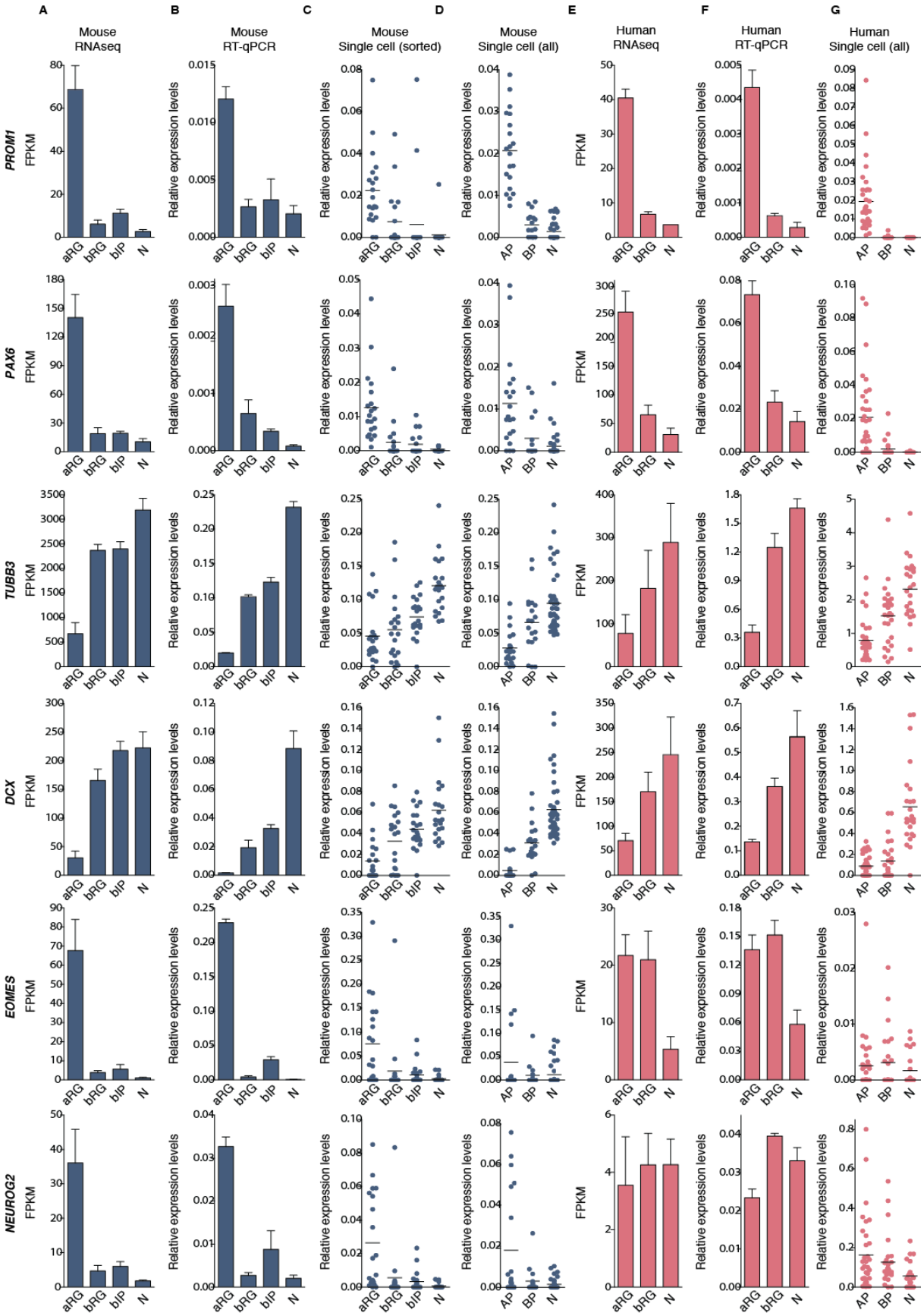
A
Mouse RNAseq
B
Mouse RT-qPCR
C
Mouse Single cell (sorted)
D
Mouse Single cell (all)
E
Human RNAseq
F
Human RT-qPCR
G
Human Single cell (all)
PROM1
PAX6
TUBB3
DCX
EOMES
NEUROG2
FPKM
Relative expression levels
aRG
bRG
bIP
N
AP
BP

Fig. S3: Validation of gene expression of known cortical progenitor and neuronal markers.

Gene expression analysis by (**A**) RNA sequencing in mouse, (**B**) RT-qPCR in mouse, (**C**) single cell RT-qPCR of purified mouse cells, (**D**) single cell RT-qPCR of unsorted and retrospectively assigned cells in mouse, (**E**) RNA sequencing in human, (**F**) RT-qPCR in human, and (**G**) single cell RT-qPCR of unsorted and retrospectively assigned cells in human. RT-PCR expression was normalized to *Gapdh*. Single cell RT-qPCR is relative to *Actb*. For assignment of unsorted cells to APs, BPs and neuron (N), see Fig. S2. Note that *Neurog2* is preferentially expressed during the G1 phase of the cell cycle, which may explain the relatively high values of NEUROG2 in the human N fraction (**E, F**); see also Fig S14.

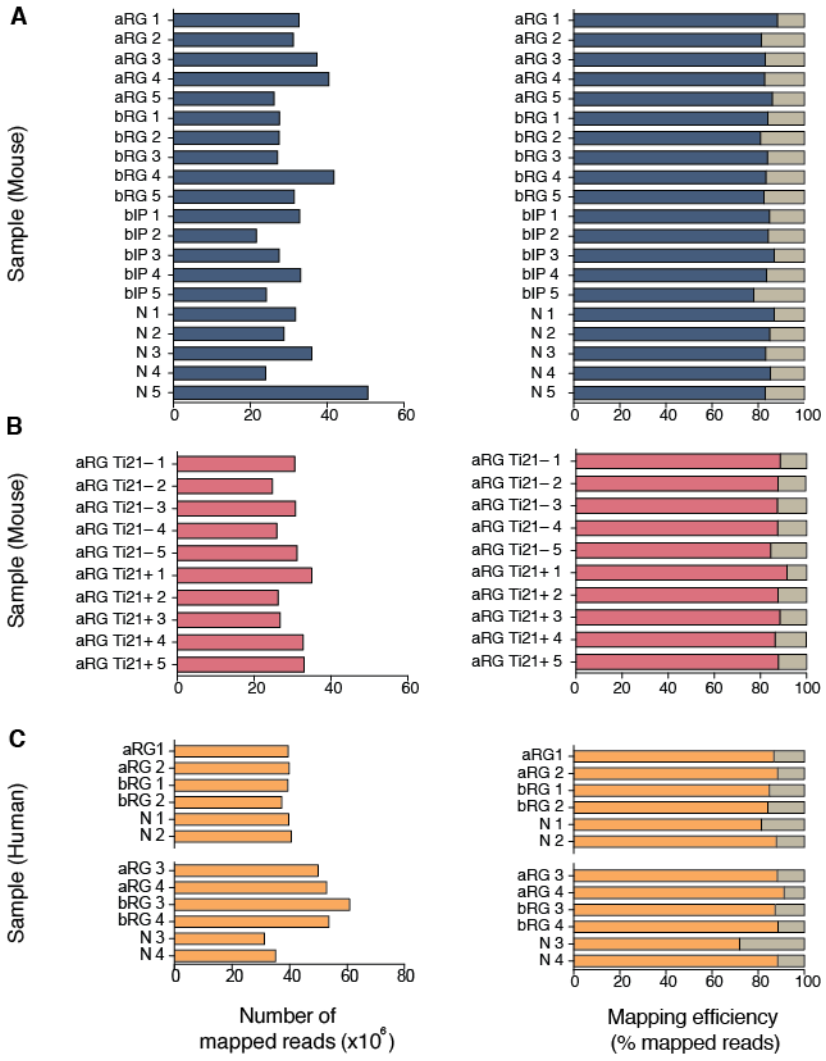

Fig. S4: Mapping efficiency of RNAseq samples.

(**A-C**) Histograms showing the total number of mapped sequencing reads (on the left) and total number of mapped reads aligned over the total number of sequencing reads (on the right) for all sequencing experiments. Sample IDs are indicated on y-axes. (**A**) Data relative to the sequencing of aRG, bRG, bIP, N_b isolated cell fractions; (**B**) data relative to the sequencing of Tis21+ and Tis21− mouse aRG fractions; (**C**) data relative to two sequence experiments (indicated by the gap on the y dimension of the plot) conducted on the isolated cell fractions from the two human samples.

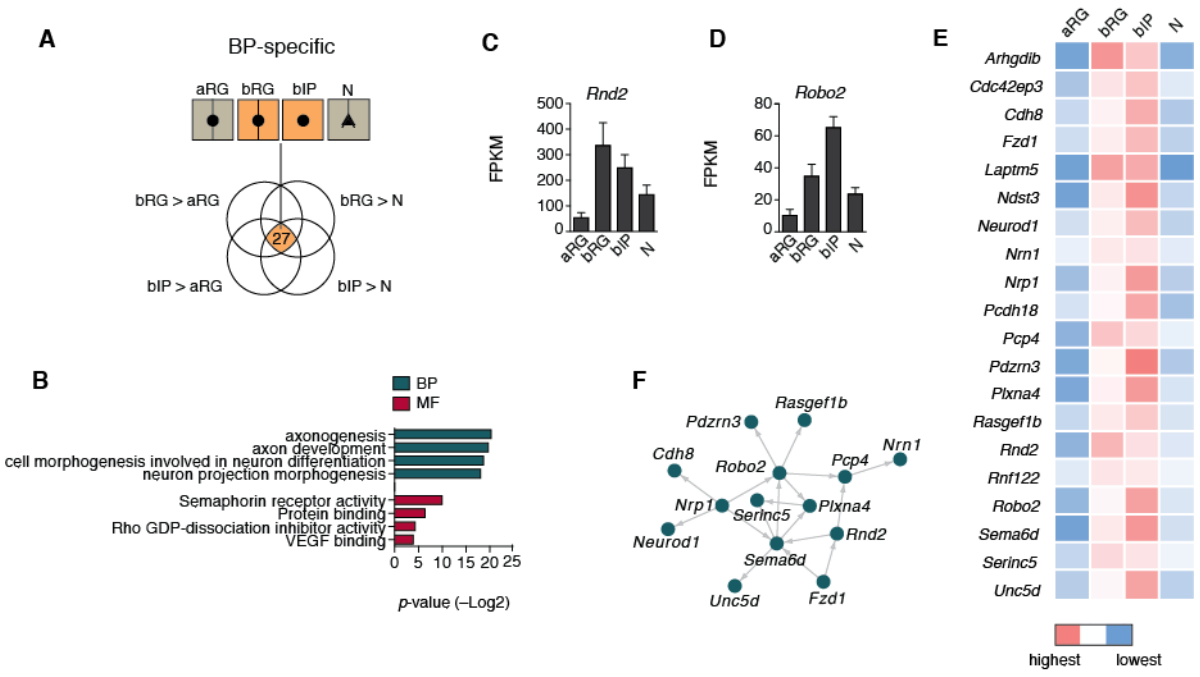

Fig. S5: A signature of neuron differentiation is a hallmark of all mouse BP subtypes.

(**A**) Venn diagram showing differential gene expression analysis carried out in mouse to reveal 27 genes up-regulated in both bRG and bIPs relative to aRG and neurons (N). Yellow, intersection between the sets of genes up-regulated ($p<0.01$) in bRG relative to both aRG and N, and in bIPs relative to both aRG and N (BP-specific gene set). (**B**) The BP-specific gene set was analyzed for significantly (p-value <0.05) enriched GO terms, which were clustered using DAVID. The 4 clusters with the highest enrichment scores are shown, for both biological process (BP) and molecular function (MF). Note the enrichment in terms associated with neuron differentiation. (**C,D**) FPKM values for Rnd2 (**C**) and Robo2 (**D**), showing the gene expression enrichment in bRG and bIPs, respectively. (**E**) Heatmap showing the relative expression levels (see color key) of 20 selected genes within the BP-specific gene set. (**F**) GO-biological process based gene network analysis, obtained using the GENEmania plugin of Cytoscape, on genes within the BP-specific gene set, showing genes within the set connected by first-order interactions.

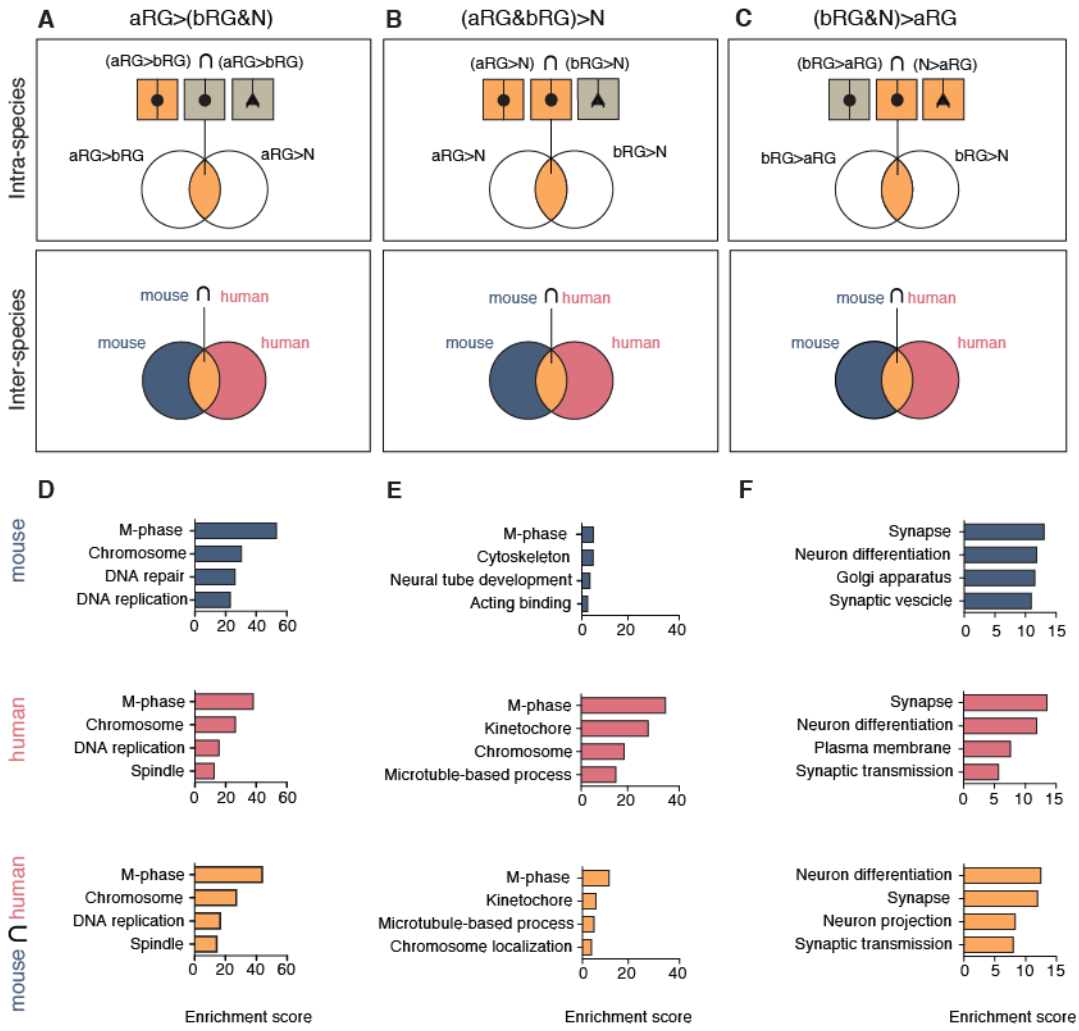

Fig. S6: Inter- and intra-species comparisons of cell-type specific gene expression profiles between mouse and human.

(**A-C**) top, Venn diagrams showing differential gene expression analysis carried out between cell types within each species, yielding the following gene sets: a, aRG specific: intersection (yellow) between the sets of genes up-regulated ($p<0.01$) in aRG relative to both bRG and N; b, aRG & bRG specific: intersection between the sets of genes up-regulated in both aRG and bRG relative to N; c, bRG & N specific, intersection between the sets of genes up-regulated in both bRG and N relative to aRG. (**A-C**) bottom, Venn diagrams showing the comparisons of each gene set identified in (**A-C** top) between mouse and human. Numbers indicate genes for which the differential gene expression patterns identified in (**A-C** top) are either observed for both mouse and human (yellow) or only observed in one of the two species (blue, red). (**D-F**), Each gene set resulting from the inter-species comparison carried out in (**A-C**, bottom) was analyzed for significantly (p-value <0.05) enriched GO terms (category: biological process), which were clustered using DAVID. The 4 clusters with the highest enrichment scores are shown.

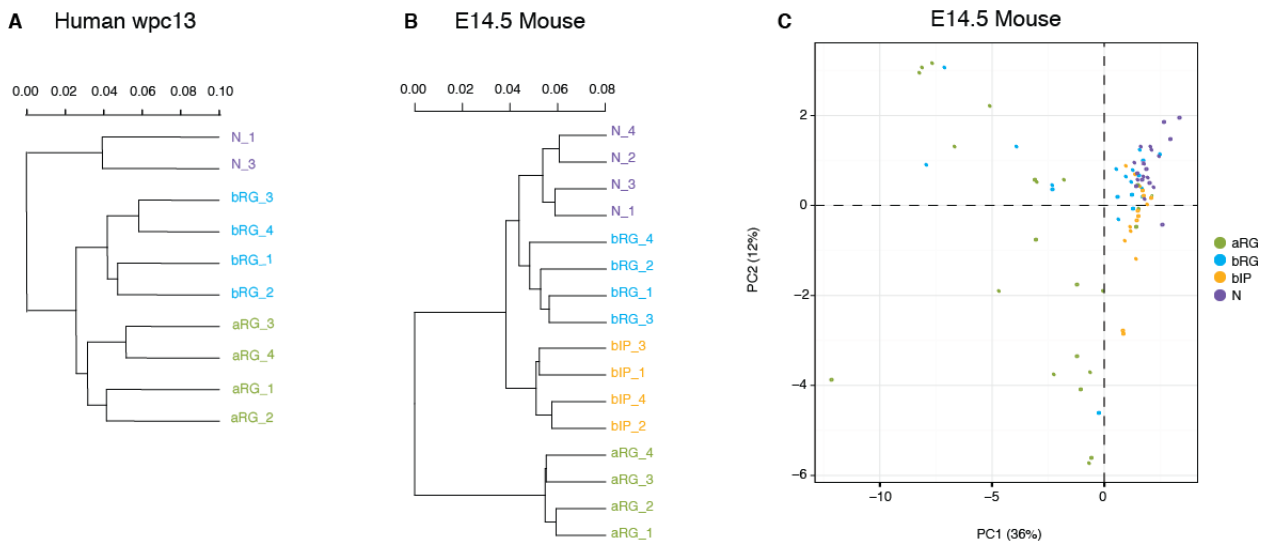

Fig. S7: Hierarchical clustering and principal component analysis of NPC subpopulation.

(**A,B**) Dendrograms showing hierarchical cluster analysis of mouse (**A**) and human (**B**) cell fractions, showing the clustering of replicates (5 for mouse, 2 for human). rs, Spearman's rank correlation coefficient. (**C**) Principle component analysis (PCA) of purified mouse cells. Mouse cells were labeled and FAC-sorted as described in Fig. S14, and analyzed by single cell RT-qPCR. The analysis included expression of 26 genes listed in Fig. S2. The PCA analysis shows that bIPs (n=19) cluster closest to neurons (N; n=21), whereas bRG (n=20) are located between aRG (n=20) and bIPs. Note that some bRG are located among the aRG population, suggesting that also in mouse a subpopulation of bRG might sustain aRG properties.

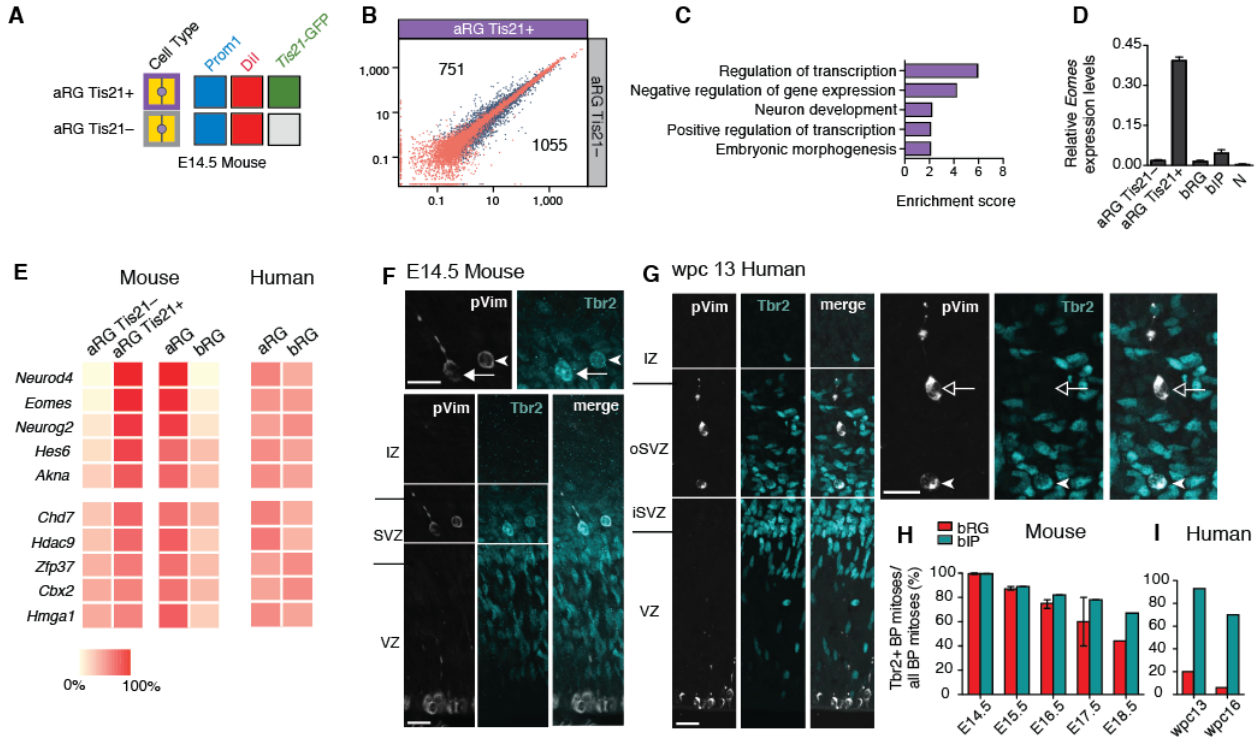

Fig. S8: Transcriptome analysis of *Tis21*-GFP– vs. *Tis21*-GFP+ aRG and comparison of *Eomes*/Tbr2 mRNA vs. protein expression in embryonic mouse and fetal human neocortex.

(**A**) Markers used to isolate *Tis21*-GFP–positive (top row) vs. –negative (bottom row) aRG (yellow boxes) by FACS from cell suspensions prepared from E14.5 *Tis21*-GFP mouse neocortex. Note that *Tis21*-GFP–positive aRG include nascent BPs not yet delaminated from the ventricular surface. (**B**) DESeq scatter plot showing comparison of the expression of protein-encoding genes between E14.5 *Tis21*-GFP–negative and –positive mouse aRG genes (mean of five independent experiments). (**C**) Clusters of GO terms (category: biological process) enriched in the 1,055 genes up-regulated in E14.5 *Tis21*-GFP–positive mouse aRG as compared to *Tis21*-GFP–negative aRG (see **B**). The 5 clusters with the highest enrichment scores are shown. Note that the GO term cluster with the highest enrichment score (Regulation of transcription) contains the Tbr2-encoding gene *Eomes*. (**D**) qPCR for *Eomes mRNA* of FACS-isolated E14.5 *Tis21*-GFP–negative and –positive mouse aRG (see **A**) and of FACS-isolated E14.5 mouse bRG, bIPs and neurons (N) (see Fig. 1B). Data show *Eomes* mRNA levels relative to *GAPDH* mRNA. Note the enrichment of *Eomes* mRNA in *Tis21*-GFP–positive aRG. (**E**) Genes up-regulated in E14.5 *Tis21*-GFP–positive mouse aRG as compared to *Tis21*-GFP–negative aRG and found in the GO term cluster with the highest enrichment score (Regulation of transcription, see **C**, 132 genes) were analyzed for their occurrence among the 1,162 genes showing E14.5 mouse aRG>bRG and 13 wpc human aRG=bRG expression (see Fig. 1H, gene set 3), which yielded 24 genes. The heatmap shows the relative expression levels (see color key) of 10 selected genes in the three pairs of cell types; top 5, transcription factors; bottom 5, epigenetic regulators. (**F-I**) Comparison of Tbr2 expression in human vs. mouse bRG. (**F, G**) Double immunofluorescence for phosphovimentin (pVim, white) and Tbr2 (cyan) on 70-µm vibratome (**F**) and 25-µm cryosections (**J**) of E14.5 mouse (**I**) and 13 wpc human (**G**) neocortex. Ventricular surface is

down; scale bars, 20 μm. Boxes indicate areas shown at higher magnification on the top and on the right; scale bars, 20 μm. Solid arrows, Tbr2+ mouse bRG; open arrows, Tbr2– human bRG; solid arrowheads, Tbr2+ bIPs. (**H-I**) Quantification of the percentage of Tbr2+ mitotic E14.5-18.5 mouse (**H**) and 13-16 wpc human (**I**) bRG and bIPs are defined by the presence or absence of a pVim+ basal process. Data are the mean or the variation of the individual values from the mean of: mouse E14.5, n=4; E15.5, n=3; E16.5, n=2; E17.5, n=2; E18.5, n=1, human: 13wpc, 16wpc, n=1 (n=one brain from an independent litter).

Description of data: We set out to explore the differences in gene expression between proliferative radial glia and radial glia committed to the neurogenic lineage. To this end, we applied our DiI/Prom1 isolation method (see Fig 1A-B) to the *Tis21*-GFP knock-in mouse line (*36*) and isolated proliferative (*Tis21*-GFP–) and differentiative (*Tis21*-GFP+) aRG (**A**). We carried out RNA-Seq on the isolated fractions (Fig. S4B), and performed differential gene expression analysis (**B**) between the two subpopulations. GO term enrichment analysis of the genes more highly expressed in Tis21-GFP+ aRG compared to Tis21-GFP– aRG (**B**) revealed a change in the regulation of transcription upon the switch from proliferative to neurogenic fate (**C**). Notably, the relative mRNA level of *Eomes*, which encodes the transcription factor Tbr2 characteristically found in mouse bIPs (*41*) was highest in *Tis21*-GFP+ aRG of the four NPC fractions analyzed, which included bIPs (**D**). See also Fig S9 and Fig S9 legend.

Not only *Eomes*, but also 23 additional genes with higher expression in *Tis21*-GFP+ than *Tis21*-GFP– aRG (**B**) and present in the GO term cluster Regulation of transcription (**C**) were found in the set of 1,162 genes with similar expression levels in human bRG and aRG but down-regulated expression in mouse bRG as compared to aRG (Fig. 1H, gene set 3). These 23 genes included numerous transcription factors with established roles in the control of the aRG-to-basal progenitor transition, as well as several epigenetic regulators (**E**), consistent with the differentiative potential of human, but not mouse, bRG.

In light of the similarly low *Eomes* mRNA levels in mouse bRG and bIPs (**D**, see also Fig. S3) and the differences in gene expression between mouse and human bRG (**E**, see also Figs S9. 1G), we re-examined the previously reported absence vs. presence of Tbr2 protein in mouse bRG (*5, 6, 23, 24*) vs. bIPs (*41*), respectively, and compared mouse and human bRG with regard to Tbr2 occurrence. We observed Tbr2 immunoreactivity not only in the vast majority of mouse bIPs, but – in contrast to a previous study (*5, 6, 23, 24*) – also of mouse bRG at mitosis, with the percentage of positive cells decreasing from 99% at E14.5 to 44% at E18.5 (**F, H**). In this respect, mouse bRG are remarkably different from 13 wpc and 16 wpc human bRG, among which only a minority showed Tbr2 immunoreactivity at mitosis (20% and 6%, respectively, **G, I**) as previously reported (*5, 6, 23, 24*). In contrast, human bIPs, like mouse bIPs, showed a high proportion of Tbr2-positive cells (**G, I**).

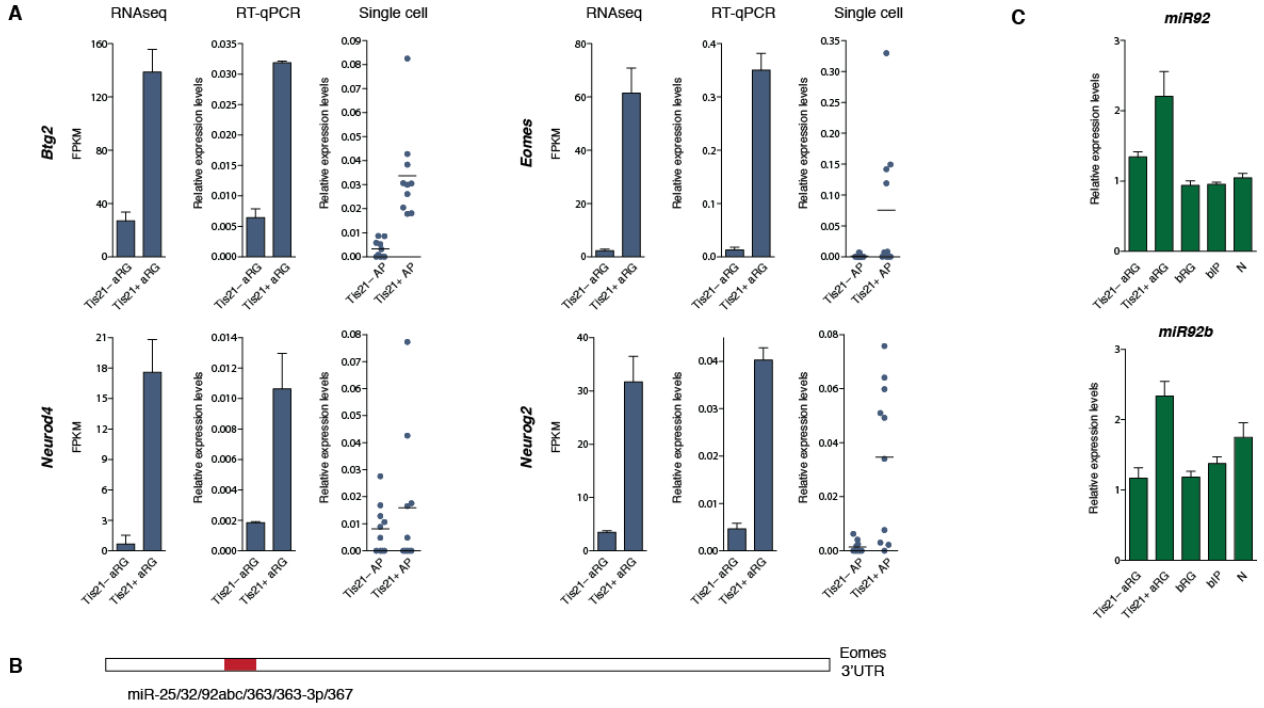

Fig. S9: Expression and regulation of *Eomes* in mouse aRGs.

(**A**) Gene expression analysis by RNA sequencing (left panels) and RT-qPCR (center panels; relative to *Gapdh*) in purified *Tis21*-GFP positive and negative aRGs, and single cell RT-qPCR (right panels; relative to *Actb*) of retrospectively classified *Tis21* positive and negative APs, for *Btg2*, *Eomes*, *NeuroD4* and *Neurog2*. (**B**) Schematic representation of predicted miRNA binding sites within the *Eomes* 3'UTR. (**C**) RT-qPCR analysis of *miR92* and *miR92b* (relative to *RNU6-2*). Note that both miRNAs have been reported to regulate Tbr2 expression in the mouse embryonic neocortex (*42, 43*) and might thus be involved in translational repression of the Eomes mRNA in aRG. Error bars represent SD of three PCR amplifications for each sample.

Description of data: Data presented in Fig. S8C-E were corroborated by single cell RT-qPCR and extended to other proneural factors related to *Eomes*, including *Neurog2* (**A**). As the vast majority of mitotic aRG lack Tbr2 protein (*41*), this finding implies inhibition of Tbr2 translation in aRG, which is then abrogated in newborn bIPs. Consistent with the expression profile of *Eomes*, we found that two microRNAs, miR92 and miR92b, previously identified as potential inhibitors of *Eomes* mRNA translation (*42, 43*), were expressed more highly in aRG than BPs, and most highly in *Tis21*-GFP+ aRG (**B, C**).

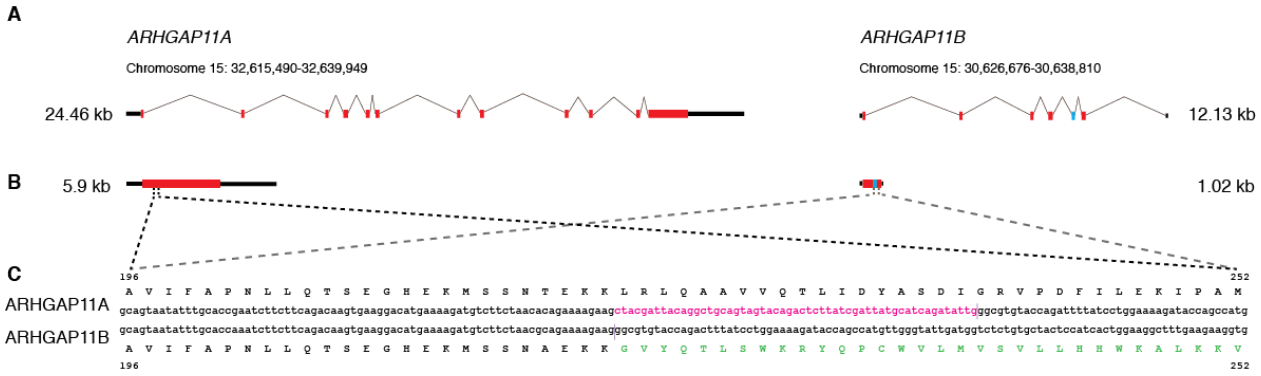

Fig. S10: Comparison of the human ARHGAP11A and ARHGAP11B gene and protein.

(**A**) The *ARHGAP11A* gene contains 12 exons spanning 24.46 kb of chromosome 15. ARHGAP11B is also located on chromosome 15, however, only contains 7 exons and spans 12.13 kb. ARHGAP11B contains a 55 nt deletion in the 3' end of exon 5 resulting in a smaller exon 5 (green). (**B**) mRNA: the 55 nt deletion in ARHGAP11B leads to a frameshift and early termination of the protein at residue 267 (exon 6). (**C**) Nucleotide sequence comparison of ARHGAP11A and ARHGAP11B around the deleted region; the deleted nucleotides are indicated by pink letters. Vertical lines indicate the exon 5 – exon 6 boundaries; note the truncation of exon 5 in ARHGAP11B and the resulting a frameshift, encoding a new amino acid sequence (green).

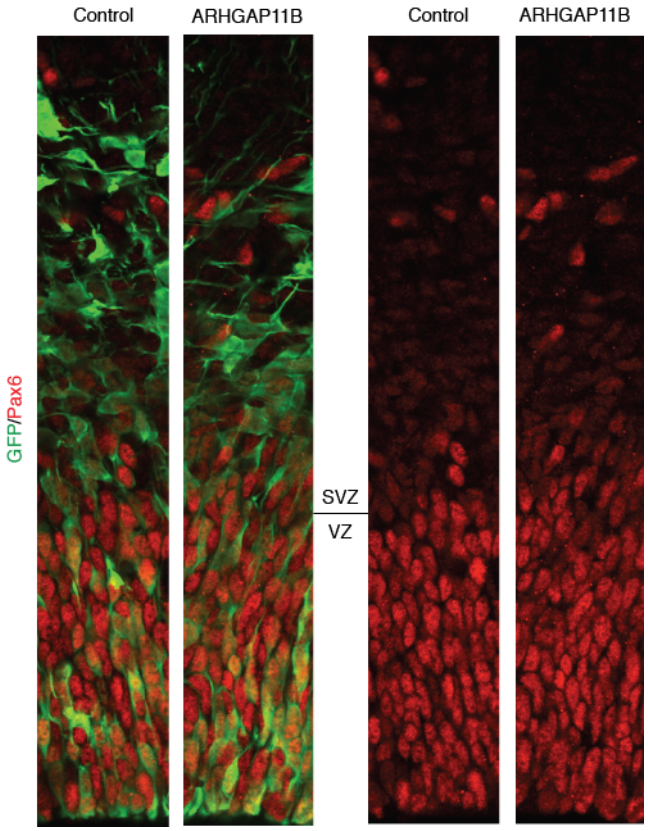

Fig. S11: ***ARHGAP11B*** **expression in mouse aRG does not alter the expression of Pax6+ in basal progenitors.**
Control and *ARHGAP11B in utero* electroporation of E13.5 mouse neocortex, followed by analysis at E14.5. Pax6 immunofluorescence (red) with (left) and without (right) GFP immunofluorescence (green).

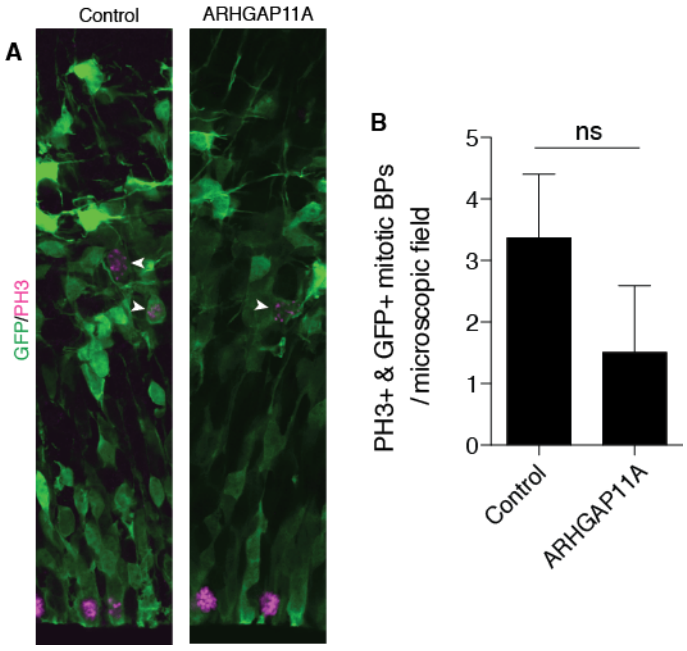

Fig. S12: ***ARHGAP11A* overexpression in mouse aRG does not increase mitotic basal progenitors**

(**A-B**) Control and *ARHGAP11A in utero* electroporation of E13.5 mouse neocortex, followed by analysis at E14.5. (**A**) GFP (green) and phosphohistone H3 (PH3, magenta) immunofluorescence; arrowheads indicate GFP+ / PH3+ basal mitoses. Single optical sections. (**B**) Quantification of mitotic, PH3+ & GFP+ basal progenitors; data are the mean of 3 independent experiments; error bars, SEM; ns, not statistically significant.

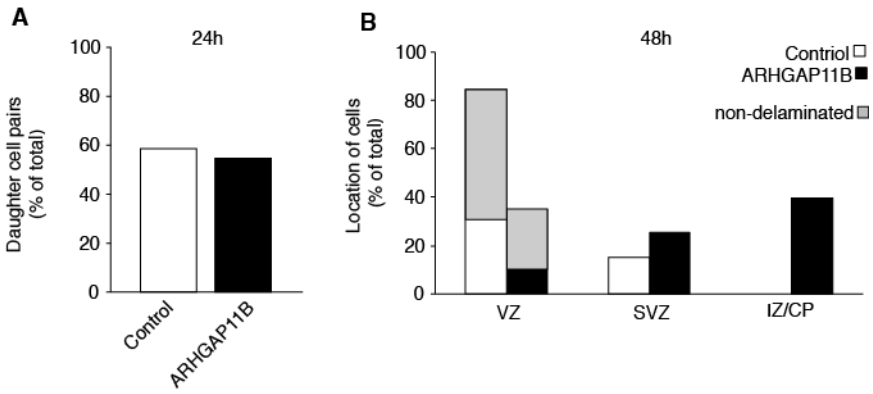

Fig. S13: Analysis of progeny number and localization upon aRG control and *ARHGAP11B* mRNA microinjection.

(A,B) aRG in organotypic slice culture of E14.5 mouse neocortex were microinjected with either in vitro transcribed *RFP* mRNA only (Control) or in vitro transcribed *RFP* plus *ARHGAP11B* mRNAs (ARHGAP11B), followed by culture for 24 hrs (**A**) or 48 hrs (**B**). (**A**) Quantification of the percentage of RFP+ cells identifiable as daughter cell pairs (total: Control, 41 cells; ARHGAP11B, 33 cells). (**B**) Quantification of the distribution of RFP+ cells in the VZ, SVZ and intermediate zone/cortical plate (IZ/CP) (total: Control, 13 cells; ARHGAP11B, 43 cells). The grey portions of the VZ columns indicate the percentage of non-delaminated cells (see Fig. 3I, grey).

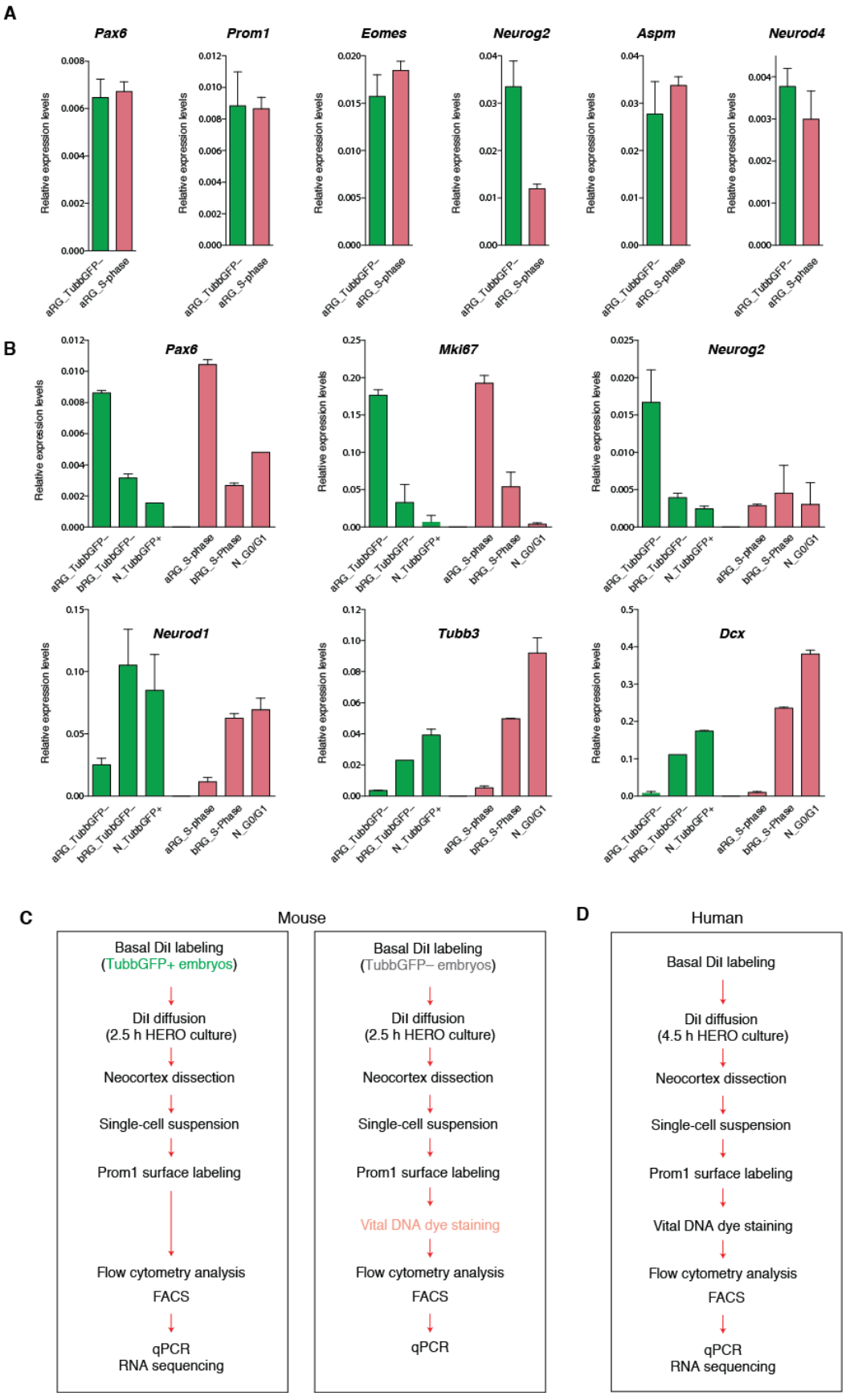
A
Pax6
Prom1
Eomes
Neurog2
Aspm
Neurod4
Relative expression levels
aRG_TubbGFP–
aRG_S-phase
B
Pax6
Mki67
Neurog2
Neurod1
Tubb3
Dcx
Relative expression levels
aRG_TubbGFP–
bRG_TubbGFP–
N_TubbGFP+
aRG_S-phase
bRG_S-Phase
N_G0/G1
C
Mouse
Basal DiI labeling
(TubbGFP+ embryos)
DiI diffusion
(2.5 h HERO culture)
Neocortex dissection
Single-cell suspension
Prom1 surface labeling
Flow cytometry analysis
FACS
qPCR
RNA sequencing
Basal DiI labeling
(TubbGFP– embryos)
DiI diffusion
(2.5 h HERO culture)
Neocortex dissection
Single-cell suspension
Prom1 surface labeling
Vital DNA dye staining
Flow cytometry analysis
FACS
qPCR
D
Human
Basal DiI labeling
DiI diffusion
(4.5 h HERO culture)
Neocortex dissection
Single-cell suspension
Prom1 surface labeling
Vital DNA dye staining
Flow cytometry analysis
FACS
qPCR
RNA sequencing

Fig. S14: Comparison of mouse and human cell isolation strategies.

RT-qPCR was performed for selected marker genes on sorted mouse E14.5 cortical cells to compare mouse and human cell isolation strategies. (**A**) Gene expression analysis of mouse aRG isolated using either the mouse (green: aRG_Tubb3-GFP–) or the human (red: aRG_S-phase) cell isolation strategy. Both aRG populations were Prom+ and basal DiI+. Expression was normalized to *Gapdh*. Note that *Neurog2* is decreased in S-phase aRG compared to total aRG, which is in agreement with its specific expression during G1-phase. (**B**) Gene expression analysis of mouse cell populations purified using either the mouse (green) or human (red) cell isolation strategy. Green: aRG (Prom+, DiI+, Tubb3-GFP–), bRG (Prom–, DiI+, Tubb3-GFP–), N (Prom–, DiI+, Tubb3-GFP+); red: aRG (Prom+, DiI+, S-phase), bRG (Prom–, DiI+, S-phase), N (Prom–, DiI+, G1/G0-phase). Expression was normalized to *Gapdh*. (**C, D**) Flow scheme of the isolation procedure. (**C**) Procedures used for mouse, (**D**) procedures used for human.

Description of data: To validate the two approaches used to isolate NPCs (Fig. 1B, left vs. right), we compared by qPCR the expression of selected marker genes in total, neuron-free, mouse apical progenitors (prominin-1+, *Tubb3*-GFP–) *versus* the tetraploid subpopulation of mouse apical progenitors (prominin-1+, duplicated DNA+) (**A**). While genes known to exhibit cell cycle-dependent expression (e.g., *Neurog2*) show some differences between the two cell populations, the expression levels of the vast majority of marker genes is very similar, if not identical, between total and tetraploid apical progenitors. This underscores that our approach of isolating cortical progenitor populations and separating them from postmitotic neurons based on DNA content is valid. Next, we compared by qPCR the expression of selected marker genes in the aRG, bRG and neuron fractions isolated from *Tubb3*-GFP transgenic mice and in the cell fractions obtained from mice by the diploid *versus* tetraploid cell approach, that is (i) tetraploid prominin-1+, basal DiI+ (aRG); (ii) tetraploid prominin-1–, basal DiI+ (bRG); (iii) diploid prominin-1–, basal DiI+ (neurons & bRG in G1) (**A-C**). The results are similar, showing that the use of the two approaches for mouse and human is valid. Our approach of isolating apical and basal radial glia that have progressed through DNA duplication in S-phase is in accordance with labeling these progenitors via their basal process contacting the basal lamina. In fact, basal process regrowth in newborn radial glia typically occurs in G1, and so cortical progenitors labeled by basally administered DiI are likely to be enriched for cells in S-G2-M.

Table S3

Fig.	Panel	Supplementary information
1	D	D, maximum intensity projections of 25 optical sections, D'-D''', projections of 10 optical sections.
	G	Each dot represents the mean expression level for a given gene, expressed in FPKM values. Only mean values ≥1 FPKM in at least one condition are shown. ***Sample size***: Data are the mean of: mouse, 5 independent experiments; human, 2 fetuses, 2 independent DiI labelings followed by cell isolations per fetus.
	I	For certain GO term clusters, the same designation was chosen (e.g. Cell cycle), although the individual genes in these clusters may be different and the enriched GO terms not necessarily identical.
2	A-B	From the dataset of human genes with the expression pattern aRG>bRG>N (**A**, dark green) or bRG≥aRG>N (**B**, dark green), genes with mouse orthologs that are expressed in E14.5 mouse cortical aRG, bRG and/or bIP (NPCs) and/or in E14.5 mouse VZ and/or SVZ (germinal zones, GZ) (*13*) were subtracted, yielding the two "Not expressed in mouse NPCs/GZ" subsets (emerald green). From each of these subsets, those genes with significant (FPKM value ≥5) expression in the 13-16 wpc human cortical plate (CP, (*13*)) were subtracted, yielding the two "No/low expression in human CP" subsets (**A, B**, hunter green). Each of these subsets of human genes was divided into two groups, depending on whether orthologous genes are present (yellow left) or absent (orange right) in the mouse genome. Human-specific, bRG≥aRG–enriched genes were then screened for those with a ratio of FPKM values bRG/N ≥10, yielding the RG-specific human gene *ARHGAP11B* (**B**, red).
	C-D	*P*-value for GO enrichment, $p<0.05$.
	F-G	***Sample size***: Data are the mean of 4 determinations (2 fetuses, 2 independent DiI labelings followed by cell isolations per fetus).
	H	qPCRs on single cells (dots), isolated from unlabeled 12 wpc human neocortex and retrospectively identified as APs, BPs or neurons (N) based on differential *PROM1, DCX* and *MAPT* mRNA levels. *ARHGAP11B* mRNA levels relative to *ACTB* mRNA are shown. Cells with expression values = 0 were not included in the expression analysis. They are represented on the x-axis of the graph.
3	A-B	ARHGAP11B: co-electroporation of p*EGFP-C1* plus pCMV-*ARHGAP11B* or pCAGGS-GFP plus pCAGGS-11B. Control: p*EGFP-C1* plus pCMV-no-insert or pCAGGS-GFP plus pCAGGS-no-insert. Control and ARHGAP11B data were analyzed in matching serial sections of electroporated neocortex along the rostro-caudal axis, in littermate embryo pairs. In each experiment, 2-5 sections per condition were analyzed. Data are expressed as absolute numbers of positive cells counted in a standardized microscopic field. ***Sample size***: Data are the mean of 3 independent experiments performed with pCMV plasmids, and 2 independent experiments performed with pCAGGS plasmids. ***Statistical test***: paired *t*-test.

	C-E	ARHGAP11B: electroporation with pCAGGS-GFP plus pCAGGS-11B. Control: pCAGGS-GFP plus pCAGGS-no-insert. ***Sample size***: Data are the mean of 3 independent experiments, 2-6 sections per experiment were analyzed and cell counts performed in a standardized microscopic field. For statistics, data of each condition from different experiments pooled together. ***Statistical test***: unpaired *t*-test.
	C,E	SVZ thickness was measured in a standardized microscopic field, and quantified as a ratio between the area of the SVZ itself (defined by nuclear composition and Tbr2 immunostaining) and the area of the entire cortical wall.
	F	Examples of RFP+ symmetric Tbr2–/Tbr2– daughter cell pairs are not shown. Left images are maximum intensity projections; all other images (higher magnification) are single optical sections.
	G	***Sample size***: Data are the mean of: Control, 41 cells, obtained from 3 independent experiments; ARHGAP11B, 33 cells, obtained from 4 independent experiments.
	H	***Sample size***: Data are the mean of: Control, 11 cell pairs, obtained from 3 independent experiments; ARHGAP11B, 8 cell pairs, obtained from 4 independent experiments.
	I	***Sample size***: Data are the mean of: Control, 13 cells, obtained from 3 independent experiments; ARHGAP11B, 47 cells, obtained from 3 independent experiments.
	J	***Sample size***: Data are the mean of: Control, 6 cells, obtained from 3 independent experiments; ARHGAP11B, 36 cells, obtained from 3 independent experiments.
4	B	***Sample size***: Data are the mean of: Control, 6 cells, obtained from 3 independent experiments; ARHGAP11B, 16 cells, obtained from 3 independent experiments.
	C	ARHGAP11B: electroporation with pCAGGS-GFP plus pCAGGS-11B. Control: pCAGGS-GFP plus pCAGGS-no-insert. Control and ARHGAP11B data were analyzed in matching serial sections of electroporated neocortex along the rostro-caudal axis, in littermate embryo pairs. ***Sample size***: Data are the mean of 4 independent experiments, 1-2 sections per experiment were analyzed. ***Statistical test***: paired *t*-test.
	D-G	ARHGAP11B: electroporation with pCAGGS-GFP plus pCAGGS-11B Images are representative of the phenotype observed in half (2/4) of the electroporated brains, each obtained in an independent experiment.

Supplementary Tables captions

Table S1 (Auxiliary File 1): 'aRG>bRG>neurons' gene set and step-wise filtering analysis.

Dataset including the human genes contained in the 'aRG>bRG>neurons' gene set, which has been used as input for the gene expression analysis shown in Figure 3A and described in Figure legend 3. The first spreadsheet (**aRG>bRG>N (190)**) lists the 190 genes significantly up-regulated ($p<0.01$) in aRG relative to bRG and neurons (N), and in bRG relative to N (Fig. 3A). First column: Ensemble Gene ID. Second column: gene set (aRG>bRG & bRG>N). Third and fourth columns: gene name and description, respectively. Fifth column: gene biotype (protein coding). Sixth column: FPKM values relative to human aRG, bRG and N. The second spreadsheet (**filtered msNPC+GZs, hCP (17)**) shows the stepwise exclusion of genes in the aRG>bRG>N gene set, and reads as follows. First column (aRG>bRG>N): names of the 190 genes contained in the aRG>bRG>N set. Second column (mNPC filtered): names of the 22 genes in the aRG>bRG>N list, which are not expressed (FPKM≤1) in none of the mouse neural progenitor cells (mNPCs), i.e. aRG, bRG or bIP, isolated in this study. Third column (mGZ filtered): names of the 18 genes in the 'mNPC filtered' list, which are not expressed (FPKM≤1) in none of the mouse germinal zones (mGZs), i.e. VZ or SVZ, isolated by Fietz et al. (*13*). Fourth column (hCP filtered): names of the 17 genes in the 'mGZ filtered' list, which are not expressed (FPKM≤1) in the human cortical plate (hCP), isolated by Fietz et al. (*13*). Fifth and sixth columns: Ensemble Gene ID and gene description, respectively. Seventh column, FPKM values relative to human aRG, bRG and N. The fourth spreadsheet (**with ms ortholog (13)**) lists the 13 genes in the 'hCP filtered' set, which have a mouse ortholog. First column: Ensemble Gene ID. Second column: gene set (aRG>bRG & bRG>N). Third and fourth columns: gene name and description, respectively. Fifth column: gene biotype (protein coding). Sixth column: FPKM values relative to human aRG, bRG and N. The fifth spreadsheet (**without ms ortholog (4)**) lists the 4 genes in the 'hCP filtered' set, which have no mouse ortholog. Columns read as indicated above.

Table S2 (Auxiliary File 2): 'bRG≥aRG>neurons' gene set and step-wise filtering analysis.

Dataset including the human genes contained in the 'bRG≥aRG>neurons' gene set, which has been used as input for the gene expression analysis shown in Figure 3B and described in Figure legend 3. The first spreadsheet (**bRG≥aRG>N (394)**) lists the 394 genes significantly up-regulated ($p<0.01$), or equally expressed, in bRG relative to aRG, and up-regulated in both aRG and bRG, relative to N (Fig. 3B). Columns read as indicated in the legend to Table S1. The second, third and fourth spreadsheets show the stepwise exclusion of genes in the bRG≥aRG>N gene set, and columns read as described in the legend to Table S1.

Table S3: Supplementary information to Figs. 1-4.

Table S4 (Auxiliary File 3): List of primers used for gene expression analysis by qPCR.

Lists of primers used for RT-qPCR on mouse (first spreadsheet) and human (second spreadsheet) isolated cells. Gene name, primer names, primer sequence, and references to previously published work (if any) are listed in the first, second, third and fourth column, respectively.

References and Notes

1. G. F. Striedter, *Principles of Brain Evolution* (Sinauer Associates, Sunderland, MA, 2005).

2. P. Rakic, Evolution of the neocortex: A perspective from developmental biology. *Nat. Rev. Neurosci.* **10**, 724–735 (2009). Medline doi:10.1038/nrn2719

3. J. H. Lui, D. V. Hansen, A. R. Kriegstein, Development and evolution of the human neocortex. *Cell* **146**, 18–36 (2011). Medline doi:10.1016/j.cell.2011.06.030

4. V. Borrell, I. Reillo, Emerging roles of neural stem cells in cerebral cortex development and evolution. *Dev. Neurobiol.* **72**, 955–971 (2012). Medline doi:10.1002/dneu.22013

5. M. Betizeau, V. Cortay, D. Patti, S. Pfister, E. Gautier, A. Bellemin-Ménard, M. Afanassieff, C. Huissoud, R. J. Douglas, H. Kennedy, C. Dehay, Precursor diversity and complexity of lineage relationships in the outer subventricular zone of the primate. *Neuron* **80**, 442–457 (2013). Medline doi:10.1016/j.neuron.2013.09.032

6. M. Florio, W. B. Huttner, Neural progenitors, neurogenesis and the evolution of the neocortex. *Development* **141**, 2182–2194 (2014). Medline doi:10.1242/dev.090571

7. V. Borrell, M. Götz, Role of radial glial cells in cerebral cortex folding. *Curr. Opin. Neurobiol.* **27**, 39–46 (2014). Medline doi:10.1016/j.conb.2014.02.007

8. T. Sun, R. F. Hevner, Growth and folding of the mammalian cerebral cortex: From molecules to malformations. *Nat. Rev. Neurosci.* **15**, 217–232 (2014). Medline doi:10.1038/nrn3707

9. E. Taverna, M. Götz, W. B. Huttner, The cell biology of neurogenesis: Toward an understanding of the development and evolution of the neocortex. *Annu. Rev. Cell Dev. Biol.* **30**, 465–502 (2014). Medline doi:10.1146/annurev-cellbio-101011-155801

10. I. H. Smart, C. Dehay, P. Giroud, M. Berland, H. Kennedy, Unique morphological features of the proliferative zones and postmitotic compartments of the neural epithelium giving rise to striate and extrastriate cortex in the monkey. *Cereb. Cortex* **12**, 37–53 (2002). Medline doi:10.1093/cercor/12.1.37

11. E. Lewitus, I. Kelava, A. T. Kalinka, P. Tomancak, W. B. Huttner, An adaptive threshold in mammalian neocortical evolution. *PLOS Biol.* **12**, e1002000 (2014). Medline doi:10.1371/journal.pbio.1002000

12. A. E. Ayoub, S. Oh, Y. Xie, J. Leng, J. Cotney, M. H. Dominguez, J. P. Noonan, P. Rakic, Transcriptional programs in transient embryonic zones of the cerebral cortex defined by high-resolution mRNA sequencing. *Proc. Natl. Acad. Sci. U.S.A.* **108**, 14950–14955 (2011). Medline doi:10.1073/pnas.1112213108

13. S. A. Fietz, R. Lachmann, H. Brandl, M. Kircher, N. Samusik, R. Schröder, N. Lakshmanaperumal, I. Henry, J. Vogt, A. Riehn, W. Distler, R. Nitsch, W. Enard, S. Pääbo, W. B. Huttner, Transcriptomes of germinal zones of human and mouse fetal neocortex suggest a role of extracellular matrix in progenitor self-renewal. *Proc. Natl. Acad. Sci. U.S.A.* **109**, 11836–11841 (2012). Medline doi:10.1073/pnas.1209647109

14. M. L. Arcila, M. Betizeau, X. A. Cambronne, E. Guzman, N. Doerflinger, F. Bouhallier, H. Zhou, B. Wu, N. Rani, D. S. Bassett, U. Borello, C. Huissoud, R. H. Goodman, C. Dehay, K. S. Kosik, Novel primate miRNAs coevolved with ancient target genes in

germinal zone-specific expression patterns. *Neuron* **81**, 1255–1262 (2014). Medline doi:10.1016/j.neuron.2014.01.017

15. J. A. Miller, S. L. Ding, S. M. Sunkin, K. A. Smith, L. Ng, A. Szafer, A. Ebbert, Z. L. Riley, J. J. Royall, K. Aiona, J. M. Arnold, C. Bennet, D. Bertagnolli, K. Brouner, S. Butler, S. Caldejon, A. Carey, C. Cuhaciyan, R. A. Dalley, N. Dee, T. A. Dolbeare, B. A. Facer, D. Feng, T. P. Fliss, G. Gee, J. Goldy, L. Gourley, B. W. Gregor, G. Gu, R. E. Howard, J. M. Jochim, C. L. Kuan, C. Lau, C. K. Lee, F. Lee, T. A. Lemon, P. Lesnar, B. McMurray, N. Mastan, N. Mosqueda, T. Naluai-Cecchini, N. K. Ngo, J. Nyhus, A. Oldre, E. Olson, J. Parente, P. D. Parker, S. E. Parry, A. Stevens, M. Pletikos, M. Reding, K. Roll, D. Sandman, M. Sarreal, S. Shapouri, N. V. Shapovalova, E. H. Shen, N. Sjoquist, C. R. Slaughterbeck, M. Smith, A. J. Sodt, D. Williams, L. Zöllei, B. Fischl, M. B. Gerstein, D. H. Geschwind, I. A. Glass, M. J. Hawrylycz, R. F. Hevner, H. Huang, A. R. Jones, J. A. Knowles, P. Levitt, J. W. Phillips, N. Sestan, P. Wohnoutka, C. Dang, A. Bernard, J. G. Hohmann, E. S. Lein, Transcriptional landscape of the prenatal human brain. *Nature* **508**, 199–206 (2014). Medline doi:10.1038/nature13185

16. Y. Arai, J. N. Pulvers, C. Haffner, B. Schilling, I. Nüsslein, F. Calegari, W. B. Huttner, Neural stem and progenitor cells shorten S-phase on commitment to neuron production. *Nat. Commun.* **2**, 154 (2011). Medline doi:10.1038/ncomms1155

17. A. Kawaguchi, T. Ikawa, T. Kasukawa, H. R. Ueda, K. Kurimoto, M. Saitou, F. Matsuzaki, Single-cell gene profiling defines differential progenitor subclasses in mammalian neurogenesis. *Development* **135**, 3113–3124 (2008). Medline doi:10.1242/dev.022616

18. A. A. Pollen, T. J. Nowakowski, J. Shuga, X. Wang, A. A. Leyrat, J. H. Lui, N. Li, L. Szpankowski, B. Fowler, P. Chen, N. Ramalingam, G. Sun, M. Thu, M. Norris, R. Lebofsky, D. Toppani, D. W. Kemp 2nd, M. Wong, B. Clerkson, B. N. Jones, S. Wu, L. Knutsson, B. Alvarado, J. Wang, L. S. Weaver, A. P. May, R. C. Jones, M. A. Unger, A. R. Kriegstein, J. A. West, Low-coverage single-cell mRNA sequencing reveals cellular heterogeneity and activated signaling pathways in developing cerebral cortex. *Nat. Biotechnol.* **32**, 1053–1058 (2014). Medline doi:10.1038/nbt.2967

19. J. H. Lui, T. J. Nowakowski, A. A. Pollen, A. Javaherian, A. R. Kriegstein, M. C. Oldham, Radial glia require PDGFD-PDGFRβ signalling in human but not mouse neocortex. *Nature* **515**, 264–268 (2014). Medline doi:10.1038/nature13973

20. S. A. Fietz, W. B. Huttner, Cortical progenitor expansion, self-renewal and neurogenesis-a polarized perspective. *Curr. Opin. Neurobiol.* **21**, 23–35 (2011). Medline doi:10.1016/j.conb.2010.10.002

21. A. Attardo, F. Calegari, W. Haubensak, M. Wilsch-Bräuninger, W. B. Huttner, Live imaging at the onset of cortical neurogenesis reveals differential appearance of the neuronal phenotype in apical versus basal progenitor progeny. *PLOS ONE* **3**, e2388 (2008). Medline doi:10.1371/journal.pone.0002388

22. S. L. Houlihan, Y. Feng, The scaffold protein Nde1 safeguards the brain genome during S phase of early neural progenitor differentiation. *eLife* **3**, e03297 (2014). Medline doi:10.7554/eLife.03297

23. A. Lukaszewicz, P. Savatier, V. Cortay, P. Giroud, C. Huissoud, M. Berland, H. Kennedy, C. Dehay, G1 phase regulation, area-specific cell cycle control, and cytoarchitectonics in the primate cortex. *Neuron* **47**, 353–364 (2005). Medline doi:10.1016/j.neuron.2005.06.032

24. X. Wang, J. W. Tsai, B. LaMonica, A. R. Kriegstein, A new subtype of progenitor cell in the mouse embryonic neocortex. *Nat. Neurosci.* **14**, 555–561 (2011). Medline doi:10.1038/nn.2807

25. B. Riley, M. Williamson, D. Collier, H. Wilkie, A. Makoff, A 3-Mb map of a large Segmental duplication overlapping the α7-nicotinic acetylcholine receptor gene (*CHRNA7*) at human 15q13-q14. *Genomics* **79**, 197–209 (2002). Medline doi:10.1006/geno.2002.6694

26. F. Antonacci, M. Y. Dennis, J. Huddleston, P. H. Sudmant, K. M. Steinberg, J. A. Rosenfeld, M. Miroballo, T. A. Graves, L. Vives, M. Malig, L. Denman, A. Raja, A. Stuart, J. Tang, B. Munson, L. G. Shaffer, C. T. Amemiya, R. K. Wilson, E. E. Eichler, Palindromic GOLGA8 core duplicons promote chromosome 15q13.3 microdeletion and evolutionary instability. *Nat. Genet.* **46**, 1293–1302 (2014). Medline doi:10.1038/ng.3120

27. Y. Kagawa, S. Matsumoto, Y. Kamioka, K. Mimori, Y. Naito, T. Ishii, D. Okuzaki, N. Nishida, S. Maeda, A. Naito, J. Kikuta, K. Nishikawa, J. Nishimura, N. Haraguchi, I. Takemasa, T. Mizushima, M. Ikeda, H. Yamamoto, M. Sekimoto, H. Ishii, Y. Doki, M. Matsuda, A. Kikuchi, M. Mori, M. Ishii, Cell cycle-dependent Rho GTPase activity dynamically regulates cancer cell motility and invasion in vivo. *PLOS ONE* **8**, e83629 (2013). Medline doi:10.1371/journal.pone.0083629

28. E. Zanin, A. Desai, I. Poser, Y. Toyoda, C. Andree, C. Moebius, M. Bickle, B. Conradt, A. Piekny, K. Oegema, A conserved RhoGAP limits M phase contractility and coordinates with microtubule asters to confine RhoA during cytokinesis. *Dev. Cell* **26**, 496–510 (2013). Medline doi:10.1016/j.devcel.2013.08.005

29. P. H. Sudmant, J. O. Kitzman, F. Antonacci, C. Alkan, M. Malig, A. Tsalenko, N. Sampas, L. Bruhn, J. Shendure, E. E. Eichler; 1000 Genomes Project, Diversity of human copy number variation and multicopy genes. *Science* **330**, 641–646 (2010). Medline doi:10.1126/science.1197005

30. M. Meyer, M. Kircher, M. T. Gansauge, H. Li, F. Racimo, S. Mallick, J. G. Schraiber, F. Jay, K. Prüfer, C. de Filippo, P. H. Sudmant, C. Alkan, Q. Fu, R. Do, N. Rohland, A. Tandon, M. Siebauer, R. E. Green, K. Bryc, A. W. Briggs, U. Stenzel, J. Dabney, J. Shendure, J. Kitzman, M. F. Hammer, M. V. Shunkov, A. P. Derevianko, N. Patterson, A. M. Andrés, E. E. Eichler, M. Slatkin, D. Reich, J. Kelso, S. Pääbo, A high-coverage genome sequence from an archaic Denisovan individual. *Science* **338**, 222–226 (2012). Medline

31. K. Prüfer, F. Racimo, N. Patterson, F. Jay, S. Sankararaman, S. Sawyer, A. Heinze, G. Renaud, P. H. Sudmant, C. de Filippo, H. Li, S. Mallick, M. Dannemann, Q. Fu, M. Kircher, M. Kuhlwilm, M. Lachmann, M. Meyer, M. Ongyerth, M. Siebauer, C. Theunert, A. Tandon, P. Moorjani, J. Pickrell, J. C. Mullikin, S. H. Vohr, R. E. Green, I. Hellmann, P. L. Johnson, H. Blanche, H. Cann, J. O. Kitzman, J. Shendure, E. E. Eichler, E. S. Lein, T. E. Bakken, L. V. Golovanova, V. B. Doronichev, M. V. Shunkov, A. P. Derevianko, B. Viola, M. Slatkin, D. Reich, J. Kelso, S. Pääbo, The complete genome

sequence of a Neanderthal from the Altai Mountains. *Nature* **505**, 43–49 (2014). Medline doi:10.1038/nature12886

32. E. Taverna, C. Haffner, R. Pepperkok, W. B. Huttner, A new approach to manipulate the fate of single neural stem cells in tissue. *Nat. Neurosci.* **15**, 329–337 (2012). Medline doi:10.1038/nn.3008

33. R. Stahl, T. Walcher, C. De Juan Romero, G. A. Pilz, S. Cappello, M. Irmler, J. M. Sanz-Aquela, J. Beckers, R. Blum, V. Borrell, M. Götz, Trnp1 regulates expansion and folding of the mammalian cerebral cortex by control of radial glial fate. *Cell* **153**, 535–549 (2013). Medline doi:10.1016/j.cell.2013.03.027

34. B. G. Rash, S. Tomasi, H. D. Lim, C. Y. Suh, F. M. Vaccarino, Cortical gyrification induced by fibroblast growth factor 2 in the mouse brain. *J. Neurosci.* **33**, 10802–10814 (2013). Medline doi:10.1523/JNEUROSCI.3621-12.2013

35. M. B. Johnson, P. P. Wang, K. D. Atabay, E. A. Murphy, R. N. Doan, J. L. Hecht, C. A. Walsh, Single-cell analysis reveals transcriptional heterogeneity of neural progenitors in human cortex. *Nat. Neurosci.* 10.1038/nn.3980 (2015).

36. W. Haubensak, A. Attardo, W. Denk, W. B. Huttner, Neurons arise in the basal neuroepithelium of the early mammalian telencephalon: A major site of neurogenesis. *Proc. Natl. Acad. Sci. U.S.A.* **101**, 3196–3201 (2004). Medline doi:10.1073/pnas.0308600100

37. J. Schenk, M. Wilsch-Bräuninger, F. Calegari, W. B. Huttner, Myosin II is required for interkinetic nuclear migration of neural progenitors. *Proc. Natl. Acad. Sci. U.S.A.* **106**, 16487–16492 (2009). Medline doi:10.1073/pnas.0908928106

38. K. Kimura, M. Ito, M. Amano, K. Chihara, Y. Fukata, M. Nakafuku, B. Yamamori, J. Feng, T. Nakano, K. Okawa, A. Iwamatsu, K. Kaibuchi, Regulation of myosin phosphatase by Rho and Rho-associated kinase (Rho-kinase). *Science* **273**, 245–248 (1996). Medline

39. J. T. Paridaen, M. Wilsch-Bräuninger, W. B. Huttner, Asymmetric inheritance of centrosome-associated primary cilium membrane directs ciliogenesis after cell division. *Cell* **155**, 333–344 (2013). Medline doi:10.1016/j.cell.2013.08.060

40. N. A. Maiorano, A. Mallamaci, Promotion of embryonic cortico-cerebral neuronogenesis by miR-124. *Neural Dev.* **4**, 40 (2009). Medline doi:10.1186/1749-8104-4-40

41. C. Englund, A. Fink, C. Lau, D. Pham, R. A. Daza, A. Bulfone, T. Kowalczyk, R. F. Hevner, Pax6, Tbr2, and Tbr1 are expressed sequentially by radial glia, intermediate progenitor cells, and postmitotic neurons in developing neocortex. *J. Neurosci.* **25**, 247–251 (2005). Medline doi:10.1523/JNEUROSCI.2899-04.2005

42. S. Bian, J. Hong, Q. Li, L. Schebelle, A. Pollock, J. L. Knauss, V. Garg, T. Sun, MicroRNA cluster miR-17-92 regulates neural stem cell expansion and transition to intermediate progenitors in the developing mouse neocortex. *Cell Reports* **3**, 1398–1406 (2013). Medline doi:10.1016/j.celrep.2013.03.037

43. T. J. Nowakowski, V. Fotaki, A. Pollock, T. Sun, T. Pratt, D. J. Price, MicroRNA-92b regulates the development of intermediate cortical progenitors in embryonic mouse brain.

Proc. Natl. Acad. Sci. U.S.A. **110**, 7056–7061 (2013). Medline
doi:10.1073/pnas.1219385110